PERGAMON

Computers and Structures 79 (2001) 1959–1976

Computers & Structures

www.elsevier.com/locate/compstruc

# Structural optimization of finite deformation elastoplasticity using continuum-based shape design sensitivity formulation

Nam Ho Kim [1], Kyung Kook Choi *, Jiun Shyan Chen [2]

*Center for Computer-Aided Design and Department of Mechanical Engineering, College of Engineering, The University of Iowa, 208 Engineering Research Facility, Iowa City, IA 52242, USA*

Received 28 November 2000; accepted 23 June 2001

**Abstract**

A continuum-based shape design sensitivity formulation and optimization method is proposed for finite deformation elastoplasticity. In response analysis, the multiplicative decomposition of the deformation gradient into elastic and plastic parts is used for the hyperelasticity-based elastoplastic constitutive model with respect to the intermediate configuration. In design sensitivity analysis, the shape variation at the undeformed configuration is taken using a design velocity concept and then is transformed to the current configuration to recover the updated Lagrangian formulation. The design sensitivity equation of the direct differentiation method is solved at each time step without iteration. The effect of using different reference frames for response analysis and sensitivity analysis is discussed in detail. The path-dependency of the sensitivity is due to the evolutions of the intermediate configuration and the internal plastic variables. A numerical example is shown to confirm the accuracy and efficiency of the proposed computational method using a vehicle bumper optimization. 

*Keywords:* Design sensitivity analysis; Material derivative; Design optimization; Elastoplasticity; Finite deformation problem

## 1. Introduction

Most gradient-based design optimization algorithms require evaluation of the performance measures, such as the cost or constraints, at the given design and the sensitivity information of these performance measures with respect to the design parameters. Accurate evaluation of the performance measure and its sensitivity information is very important for stability and rapid convergence of an optimization algorithm. As engineering problems becoming more complicated, the cost of response analysis increases in spite of increased computing capability. If the conventional finite difference method is used to obtain the sensitivity information, the cost of the sensitivity computation increases tremendously; proportional to the number of design parameters. In addition to the systematic design optimization, design sensitivity information also provides useful quantitative information to the design engineer about the direction of the desired design change. In this paper, an accurate and efficient method is proposed to obtain the sensitivity information for nonlinear structural design problems.

Since many engineering applications involve plastic deformation, the design sensitivity of this application area has gained significant interest in recent years. In response analysis of plastic deformation, the return-mapping projection of the elastic trial stress is carried out to meet the variational inequality through iterations in the deviatoric stress space. The design sensitivity analysis (DSA), on the other hand, computes the rate of change of the projected solution to the response analysis

* Corresponding author. Tel.: +1-319-335-3380; fax: +1-319-335-5669.

*E-mail addresses:* nkim@ccad.uiowa.edu (N.H. Kim), kkchoi@ccad.uiowa.edu (K.K. Choi), jschen@icaen.uiowa.edu (J.S. Chen).

[1] Tel.: +1-319-335-0676; fax: +1-319-335-3380.

[2] Tel.: +1-319-335-5677; fax: +1-319-335-5669.

0045-7949/01/$ - see front matter 
PII: S0045-7949(01)00122-5

**Nomenclature**

| | | | |
|---|---|---|---|
| $\boldsymbol{b}^{e}$ | elastic left Cauchy–Green deformation tensor | $\bar{\boldsymbol{z}}$ | variation of displacement |
| $\boldsymbol{c}$ | fourth order spatial stiffness tensor | $Z$ | space of kinematically admissible displacements |
| $\boldsymbol{c}^{e}$ | second order elastic stiffness tensor in principal space | $\boldsymbol{\alpha}$ | principal back stress |
| $\boldsymbol{c}^{alg}$ | algorithmic tangent stiffness tensor | $\boldsymbol{\varepsilon}$ | engineering strain at the current configuration |
| $\boldsymbol{C}$ | fourth order material stiffness tensor | $\boldsymbol{\varepsilon}_{V}$ | explicitly dependent term of $\varepsilon$ |
| $\boldsymbol{e}$ | principal logarithmic strain | $\boldsymbol{\varepsilon}_{P}$ | path dependent term of $\varepsilon$ |
| $e^{p}$ | effective plastic strain | $\gamma$ | plastic consistency parameter |
| $E$ | elastic domain | $\Gamma$ | boundary of structural domain |
| $\boldsymbol{E}$ | Lagrangian strain tensor | $\boldsymbol{\eta}$ | nonlinear strain tensor |
| $f$ | yield function | $\boldsymbol{\eta}_{V}$ | explicitly dependent term of $\boldsymbol{\eta}$ |
| $\boldsymbol{f}(\boldsymbol{x})$ | incremental deformation gradient | $\boldsymbol{\eta}_{P}$ | path dependent term of $\boldsymbol{\eta}$ |
| $\boldsymbol{F}(\boldsymbol{X})$ | deformation gradient | $\kappa(e^{p})$ | radius of the yield surface |
| $\boldsymbol{F}^{e}(\boldsymbol{X})$ | elastic deformation gradient | $\lambda$, $\mu$ | Lame's constants |
| $\boldsymbol{F}^{p}(\boldsymbol{X})$ | plastic deformation gradient | $\boldsymbol{\sigma}$ | Cauchy stress tensor |
| $H_{\alpha}$ | plastic modulus for the kinematic hardening | $\boldsymbol{\tau}$ | Kirchhoff stress tensor |
| $\boldsymbol{I}$ | second order identity tensor | $\boldsymbol{\tau}^{p}$ | principal Kirchhoff stress vector |
| $\boldsymbol{I}_{dev}$ | second order deviatoric identity tensor | $\Omega$ | structural domain |
| $\boldsymbol{n}^{i}$ | principal direction of trial $\mathbf{b}^{e}$ | $\psi$ | free energy function |
| $\boldsymbol{N}$ | outward unit normal to the yield surface | $\Psi$ | performance measure |
| $\boldsymbol{s}$ | deviatoric principal Kirchhoff stress vector | $\mathbf{1}$ | $=[1, 1, 1]^{T}$ |
| $\boldsymbol{S}$ | second Kirchhoff stress tensor | $a_{\Omega}(\cdot,\cdot)$ | structural energy form |
| $\boldsymbol{T}$ | mapping of shape perturbation | $a^{*}_{\Omega}(\mathbf{z};\cdot,\cdot)$ | structural bilinear form |
| $\boldsymbol{V}(\boldsymbol{X})$ | design velocity field | $a'_{V}(\cdot,\cdot)$ | structural fictitious load form |
| $\boldsymbol{x}$ | material point in the deformed geometry | $\ell_{\Omega}(\cdot)$ | load linear form |
| $\boldsymbol{X}$ | material point in the undeformed geometry | $\ell'_{V}(\cdot)$ | external fictitious load |
| $\boldsymbol{z}$ | displacement function | $\nabla_{0}$ | $=\partial/\partial\boldsymbol{X}$ |
| $\dot{\boldsymbol{z}}$ | material derivative of displacement | $\nabla_{n}$ | $=\partial/\partial\boldsymbol{x}$ |

in the tangential direction of the constraint set without the need of iteration. It is important to note that the sensitivity analysis is linear and is computed without iteration even if the response analysis is nonlinear. Although rigorous mathematical studies in DSA for linear problems have been made [1], many research results were published for nonlinear problems without a mathematical proof regarding the existence and uniqueness of the design sensitivity.

Unlike the nonlinear elastic problem, the sensitivity equation of the elastoplastic problem requires the sensitivity information of the stress and the internal variables at the previous time step. The sensitivity equation is solved at each time step, and the sensitivity information of the stresses and evolution variables are updated for the design sensitivity computation at the next time step. The sensitivity equation at each load step computes material derivatives of incremental displacements. The material derivatives of total displacements are then obtained by summing up material derivatives of incremental displacements. Recently, several research results were reported regarding DSA of elastoplastic material with infinitesimal deformation, using the hypo-elastic constitutive model. Accurate sensitivity results were obtained by consistently following response analysis procedures and using the return-mapping algorithm and algorithmic tangent operator. Vidal and Haber [2] discussed the accuracy of the sensitivity coefficients with respect to the consistent tangent operator and the rate form tangent operator. For the major research results of DSA in infinitesimal elastoplasticity, refer to Refs. [2–8].

When the structure experiences large deformation, the classical theory of elastoplasticity with infinitesimal deformation assumption is modified to account for a rigid body rotation. The objective stress rate plays an important role in an elastoplasticity problem to correctly represent the rigid body motion. Efficient numerical integration that preserves stress objectivity for hypo-elastic constitutive model is highly desirable, but yet not fully developed. Further, the tangent operator that is not consistent with the integration of stress rate leads to errors in DSA.

For the finite deformation elastoplastic problem with a hypo-elastic constitutive model, it is difficult to linearize the variational equation consistently because of the rigid body rotation. An incrementally objective integration method is advocated by Hughes and Windget [9], but the consistent linearization of an objective integration method is not a trivial procedure. This lack of consistent tangent stiffness induces iteration in the sensitivity equation as experienced by Zhang et al. [10] and Dutta [11]. For the case of the explicit method, since the reference frame is at the previous configuration, Kleiber [12] and Cho and Choi [13] succeeded in solving a sensitivity equation without iteration.

On the other hand, relatively simple expressions of the design sensitivity can be obtained for the steady state problem. Maniatty and Chen [14] developed a design sensitivity formulation for the steady state metal-forming process using a semi-analytical adjoint variable method. Zao et al. [15] solved an unconstrained optimization problem to minimize the difference between the final shape of the workpiece and the desired shape. Balagangadhar and Tortorelli [16] discussed design optimization of steady state manufacturing process using a reference frame approach. However, these approaches cannot easily evaluate the residual stress and spring-back phenomena at the end of the process since rigid–plastic constitutive model is used.

An effective approach for finite deformation elastoplasticity is to consider a hyperelastic constitutive relation for the elastic response of elastoplasticity. This method defines a stress-free intermediate configuration composed of the plastic deformation, and the stress can be obtained simply by taking the derivative of the strain energy density function with reference to the intermediate configuration. Without errors involved in stress integration, an enhanced accuracy is obtained for problems with a large elastic deformation. In addition, the same return-mapping algorithm as that of the classical theory can be used in the principal stress space. Moreover, the consistent tangent stiffness guarantees the quadratic convergence in response analysis, and it provides accuracy in DSA results. The theory of the multiplicative plasticity is proposed by Lee [17] to go beyond the assumption of the small elastic strain in the theory of the classical infinitesimal plasticity, which uses an additive decomposition of the strain rate. This model is suited for the single-crystal metal plasticity (see Ref. [18]). A computational framework of this theory is proposed by Simo [19], which preserves the conventional return-mapping algorithm in the principal stress space. For major research results of finite deformation elastoplasticity with multiplicative decomposition of deformation gradient, refer to Refs. [17–24].

The Lagrangian formulation of DSA for multiplicative elastoplasticity was developed by Badrinarayanan and Zabaras [25] for die and process design. However, since the structural domain is fixed in their parameter DSA, complex transformation to the undeformed configuration does not appear. In addition, they indicated that the tangent stiffness matrix of response analysis is different from that of the design sensitivity equation, and thus another tangent stiffness matrix is computed for DSA, which reduces the computational efficiency. Recently, Wiechmann and Barthold [26] derived a sensitivity formulation that leads to the same tangent stiffness matrix as response analysis through a consistent linearization. They transform all deformation configurations into the parameter space where design variation is taken. In this case, design velocity field has to be defined at the parameter space, not at the initial structural domain. If the mapping relation between parameter space and initial domain is not specified, this approach could yield difficulty in design procedures. Thus, it is necessary to develop shape DSA that uses design velocity information at the initial undeformed domain.

A continuum-based shape DSA for finite deformation elastoplasticity with a multiplicative decomposition of the deformation gradient is developed in this paper. The spatial description of the variational equation is transformed to the undeformed configuration by a "pull-back" operation. After taking the material derivative with respect to the shape design parameters, the spatial description is recovered by a "push-forward" operation to the current configuration. This procedure is necessary since the design parameters are defined in the undeformed coordinate of the domain. It has been discussed in Ref. [19] that the specification of the intermediate configuration allows an arbitrary rigid body rotation. It is shown in this study, however, that the sensitivity of elastic rotation is not negligible and needs to be identified for sensitivity purpose.

In general, nonlinear finite deformation problems mentioned above experience very large deformation. An effective numerical method, which can handle mesh distortion problem in conventional FEA is highly desirable in analyzing finite deformation problems. In addition, even if the original mesh shape is regular enough, the mesh distortion by domain change during the shape optimization poses difficulty in obtaining stable and convergent solution. A number of meshfree methods that do not require explicit meshes in domain discretization have been proposed to alleviate the dependence of numerical solution on the quality of mesh. Belytschko et al. [27] proposed the element-free Galerkin (EFG) method based on a moving least-square approximation. Duarte and Oden [28] developed the HP Clouds method for hp-adaptivity based on the partition of unity [29]. Liu et al. [30] developed the reproducing kernel particle method (RKPM) by introducing a modified kernel function that meets reproducing conditions. The RKPM was further extended to highly nonlinear hyperelastic and elastoplastic problem by Chen

et al. [31,32]. The continuum-based variational equation of response analysis and DSA are discretized using RKPM in this work to take these advantages of the meshfree method for large deformation analysis and shape design optimization.

In this study, the response analysis is formulated meshfree discretization of the variational equation. The material derivative of this variational form is obtained using the concept of design velocity field to describe shape design changes of the structural system. The shape sensitivity expression obtained from the structural variational form depends on the domain design velocity. By solving linear system of the sensitivity equation, the design sensitivity of a displacement performance measure can be obtained. The sensitivities of the performance measures such as stress and reaction force are obtained using the direct differentiation method (DDM) in this paper. Since the stress and reaction force performance measures depend on the shape design variable implicitly through the displacement, the design sensitivity of the displacement is used to obtain the design sensitivity of the performance measure.

The feasibility of the proposed methods is demonstrated through the design optimization of a vehicle bumper contact problem. The design sensitivity results are compared with the finite difference results, and excellent agreements are observed. The cost of computing sensitivity information is shown to be very small compared with that of response analysis and thus, the finite difference method.

## 2. Review of response analysis using multiplicative elastoplasticity in finite deformation

Many difficulties regarding the finite deformation in plasticity can be resolved by using a phenomenological model where the constitutive equation is formulated in a hyperelasticity typed relationship. The multiplicative decomposition of elastic–plastic deformation is converted into additive decomposition by defining appropriate stress and strain measures. In the DSA point of view, this formulation yields the *total form* of the design sensitivity equation compared to the incremental form in classical elastoplastic response analysis. A major difficulty in DSA is due to the fact that the design parameters are referenced to the undeformed configuration, whereas the reference for response analysis is the stress-free intermediate configuration. The design sensitivity of intermediate configuration needs to be stored and updated at each load step.

### 2.1. Finite deformation elastoplasticity

In this section, the constitutive relation of multiplicative plasticity [18] and the associated computational method using return-mapping algorithm [19] are summarized. Let $\boldsymbol{X}$ be the material point in the initial domain, and its position in the current configuration is denoted by $\boldsymbol{x} = \boldsymbol{X} + \boldsymbol{z}$, where $\boldsymbol{z}$ is the displacement. The deformation gradient $\boldsymbol{F}(\boldsymbol{X})$ of the material point $\boldsymbol{X}$ is assumed to take the form of local multiplicative decomposition as follows:

$$\boldsymbol{F}(\boldsymbol{X}) = \boldsymbol{F}^{\mathrm{e}}(\boldsymbol{X})\boldsymbol{F}^{\mathrm{p}}(\boldsymbol{X}) \tag{1}$$

where $\boldsymbol{F}^{\mathrm{p}}(\boldsymbol{X})$ denotes the plastic deformation at the stress-free intermediate configuration that is defined through an elastic unloading process $\boldsymbol{F}^{\mathrm{e}^{-1}}(\boldsymbol{X})$. The elastic stress domain is defined using a Kirchhoff stress tensor, $\boldsymbol{\tau} = \boldsymbol{\sigma}\det(\boldsymbol{F})$ and the stress-like internal variable $\boldsymbol{q}$, as

$$E \equiv \{(\boldsymbol{\tau}, \boldsymbol{q}) | f(\boldsymbol{\tau}, \boldsymbol{q}) \leqslant 0\} \tag{2}$$

where $\boldsymbol{\sigma}$ is the Cauchy stress and $f$ the yield function. The yield potential function $f(\boldsymbol{\tau}, \boldsymbol{q})$ of Eq. (2) is an isotropic function of $\boldsymbol{\sigma}$ due to the principle of objectivity. That is, the yield potential function does not depend on the orientation of the stress or internal variables. It is assumed that the free energy function depends locally on $\boldsymbol{F}^{\mathrm{e}}(\boldsymbol{X})$ only, since the free energy represents the stored energy through the elastic deformation. In addition, the free energy function is independent of the orientation, like the yield potential function, as

$$\psi = \psi(\boldsymbol{b}^{\mathrm{e}}, \boldsymbol{\xi}) \tag{3}$$

where $\boldsymbol{b}^{\mathrm{e}} \equiv \boldsymbol{F}^{\mathrm{e}}\boldsymbol{F}^{\mathrm{e}^{\mathrm{T}}}$ is the elastic left Cauchy–Green deformation tensor and $\boldsymbol{\xi}$ is the vector of strain-like internal variables that is conjugate to $\boldsymbol{q}$ in the sense that $\boldsymbol{q} \equiv -\partial\psi/\partial\boldsymbol{\xi}$.

For the displacement-controlled problem, the deformation state $\{\boldsymbol{F}_n, \boldsymbol{b}_n^{\mathrm{e}}, \boldsymbol{\xi}_n\}$ at time $t_n$ and the incremental displacement $\Delta\boldsymbol{z}$ are known. The objective is to obtain the current deformation that satisfies all the constitutive and evolution equations. The relative deformation gradient from time $t_n$ to $t_{n+1}$ is defined as

$$\boldsymbol{f}(\boldsymbol{x}) = \boldsymbol{I} + \nabla_n(\Delta\boldsymbol{z}) \tag{4}$$

The total deformation gradient at time $t_{n+1}$ is then $\boldsymbol{F}_{n+1}(\boldsymbol{X}) = \boldsymbol{f}(\boldsymbol{x})\boldsymbol{F}_n(\boldsymbol{X})$.

In computation, the elastoplastic evolution can be described by an elastic trial state and a plastic return mapping. The elastic trial state can be obtained by eliminating the plastic flow and pushing forward the elastic left Cauchy–Green deformation tensor to the current configuration using the relative deformation gradient as

$$\boldsymbol{b}^{\mathrm{e}^{\mathrm{tr}}} = \boldsymbol{f}\boldsymbol{b}_n^{\mathrm{e}}\boldsymbol{f}^{\mathrm{T}}, \quad \boldsymbol{\xi}^{\mathrm{tr}} = \boldsymbol{\xi}_n \tag{5}$$

For the given trial state, the deformation tensor can be represented by the spectral decomposition as

$$\boldsymbol{b}^{\mathrm{e^{tr}}} = \sum_{i=1}^{3} v_i^{\mathrm{tr}^2} \boldsymbol{n}^i \otimes \boldsymbol{n}^i \tag{6}$$

where $v_i^{\mathrm{tr}}$ is the principal stretch and $\boldsymbol{n}^i$ is the principal direction. For simplicity, vector notations are defined as follows. A logarithmic elastic principal stretch and principal stress vectors are defined by $\boldsymbol{e} = [e_1, e_2, e_3]^{\mathrm{T}} = [\log(v_1), \log(v_2), \log(v_3)]^{\mathrm{T}}$ and $\boldsymbol{\tau}^{\mathrm{p}} = [\tau_1^{\mathrm{p}}, \tau_2^{\mathrm{p}}, \tau_3^{\mathrm{p}}]^{\mathrm{T}}$, respectively. The relation between the elastic trial principal stress and the logarithmic principal elastic stretch is

$$(\boldsymbol{\tau}^{\mathrm{p}})^{\mathrm{tr}} = \boldsymbol{c}^{\mathrm{e}} \boldsymbol{e}^{\mathrm{tr}} \tag{7}$$

where $\boldsymbol{c}^{\mathrm{e}} = (\lambda + \frac{2}{3}\mu)\mathbf{1} \otimes \mathbf{1} + 2\mu \boldsymbol{I}_{\mathrm{dev}}$ is the usual $3 \times 3$ elasticity tensor for an isotropic material, $\mathbf{1} = [1, 1, 1]^{\mathrm{T}}$, $\boldsymbol{I}_{\mathrm{dev}} = \boldsymbol{I} - (\mathbf{1} \otimes \mathbf{1})/3$, and $\lambda$ and $\mu$ are Lame's constants. From the isotropic assumption, the principal direction of $\boldsymbol{\tau}$ is coincided to that of $\boldsymbol{b}^{\mathrm{e}}$, thus

$$\boldsymbol{\tau}^{\mathrm{tr}} = \sum_{i=1}^{3} \tau_i^{\mathrm{p^{tr}}} \boldsymbol{n}^i \otimes \boldsymbol{n}^i \tag{8}$$

If $\boldsymbol{\tau}$, evaluated using the trial state in Eq. (8), is within the elastic domain of Eq. (2), then the trial stress in Eq. (8) exacts. Otherwise, the plastic return mapping is carried out along the fixed principal direction. The return-mapping procedures are listed below

$$\begin{aligned} &\boldsymbol{\tau}_{n+1}^{\mathrm{p}} = (\boldsymbol{\tau}^{\mathrm{p}})^{\mathrm{tr}} - \gamma \boldsymbol{c}^{\mathrm{e}} \frac{\partial f(\boldsymbol{\tau}^{\mathrm{p}}, \boldsymbol{q})}{\partial \boldsymbol{\tau}^{\mathrm{p}}} \\ &\boldsymbol{\xi}_{n+1} = \boldsymbol{\xi}_n + \gamma \frac{\partial f(\boldsymbol{\tau}^{\mathrm{p}}, \boldsymbol{q})}{\partial \boldsymbol{q}} \\ &\gamma \geqslant 0, \quad f(\boldsymbol{\tau}^{\mathrm{p}}, \boldsymbol{q}) \leqslant 0, \quad \gamma f(\boldsymbol{\tau}^{\mathrm{p}}, \boldsymbol{q}) = 0 \end{aligned} \tag{9}$$

where $\gamma$ is the consistency parameter. The return-mapping algorithms in Eq. (9) are with the same forms as those of the classical plasticity. The only difference is that the principal Kirchhoff stress and logarithmic strain are used instead of the Cauchy stress and engineering strain.

### 2.2. Return mapping algorithms for isotropic/kinematic hardening materials

Since the plastic behavior can be efficiently described by the deviator of stresses, the deviatoric principal stress is defined by

$$\boldsymbol{s} \equiv \boldsymbol{\tau}^{\mathrm{p}} - \frac{1}{3}(\boldsymbol{\tau}^{\mathrm{p}} \cdot \mathbf{1})\mathbf{1} \tag{10}$$

For rate independent plasticity, the von Mises pressure insensitive yield criterion and the associative flow rule are commonly used for discretizing elastoplastic behavior of metal-like material. The yield function is given as

$$f(\boldsymbol{\eta}, e^{\mathrm{p}}) = \|\boldsymbol{\eta}\| - \sqrt{\frac{2}{3}}\kappa(e^{\mathrm{p}}) = 0 \tag{11}$$

where $\boldsymbol{\eta} = \boldsymbol{s} - \boldsymbol{\alpha}(e^{\mathrm{p}})$ and $\boldsymbol{\alpha}(e^{\mathrm{p}})$ is the back stress. In Eq. (11), $\kappa(e^{\mathrm{p}})$ is the radius of the yield surface and determined by the isotropic hardening rule. The internal variables are reduced to the effective plastic strain $e^{\mathrm{p}}$ and the back stress.

The return-mapping algorithm in the principal Kirchhoff stress space is

$$\begin{aligned} &\boldsymbol{\tau}_{n+1}^{\mathrm{p}} = (\boldsymbol{\tau}^{\mathrm{p}})^{\mathrm{tr}} - 2\mu\gamma \boldsymbol{N} \\ &\boldsymbol{\alpha}_{n+1} = \boldsymbol{\alpha}_n + \gamma H_\alpha(e^{\mathrm{p}}) \boldsymbol{N} \\ &e_{n+1}^{\mathrm{p}} = e_n^{\mathrm{p}} + \sqrt{\frac{2}{3}}\gamma \end{aligned} \tag{12}$$

where $H_\alpha(e^{\mathrm{p}})$ is a plastic modulus for the kinematic hardening and

$$\boldsymbol{N} \equiv \frac{\boldsymbol{\eta}}{\|\boldsymbol{\eta}\|} = \frac{\boldsymbol{\eta}^{\mathrm{tr}}}{\|\boldsymbol{\eta}^{\mathrm{tr}}\|} \tag{13}$$

is an outward unit normal to the yield surface. In Eq. (12), $\gamma$ is computed using a local Newton–Raphson method by imposing the following consistency condition

$$\begin{aligned} f(\boldsymbol{\eta}, e^{\mathrm{p}}) &= \|\boldsymbol{\eta}\| - \sqrt{\frac{2}{3}}\kappa(e^{\mathrm{p}}) \\ &= \|\boldsymbol{\eta}^{\mathrm{tr}}\| - [2\mu + H_\alpha(e^{\mathrm{p}})]\gamma - \sqrt{\frac{2}{3}}\kappa(e^{\mathrm{p}}) = 0 \end{aligned} \tag{14}$$

which is in general a nonlinear equation in $\gamma$. The convexity of the elastic domain guarantees the stability of the return-mapping algorithm. If the isotropic/kinematic hardening is a linear function of $\gamma$ or the effective plastic strain, then only one iteration is required to compute the return map point. The gradient of $f$ in Eq. (14) can be evaluated by

$$\frac{\partial f}{\partial \gamma} = -\left(2\mu + H_\alpha + \sqrt{\frac{2}{3}}H'_\alpha \gamma + \frac{2}{3}\kappa'\right) \equiv -\frac{1}{A} \tag{15}$$

The Kirchhoff stress tensor can be obtained from Eq. (8) using the principal stress and principal direction as

$$\boldsymbol{\tau} = \sum_{i=1}^{3} \tau_i^{\mathrm{p}} \boldsymbol{m}^i, \quad \text{where } \boldsymbol{m}^i = \boldsymbol{n}^i \otimes \boldsymbol{n}^i \tag{16}$$

The left Cauchy–Green deformation tensor is updated using the formula in Eq. (6), which represents the intermediate configuration

$$\boldsymbol{b}^{\mathrm{e}} = \sum_{i=1}^{3} \exp(2e_i) \boldsymbol{n}^i \otimes \boldsymbol{n}^i \tag{17}$$

where $e = e^{\mathrm{tr}} - \gamma N$ is the elastic logarithmic principal strain.

### 2.3. Consistent algorithmic tangent operator

The consistent tangent operator can be obtained by taking the derivative of the Kirchhoff stress tensor in Eq. (16) with respect to the strain. This spatial tangent operator is related with the material tangent operator by

$$c_{mnst} = F_{mI}F_{nJ}F_{sK}F_{tL}C_{IJKL} \tag{18}$$

where $C_{IJKL} = \partial S_{IJ}/\partial E_{KL}$ is the material response tensor, $E_{KL}$ is a component of Lagrangian strain tensor, and $S_{IJ}$ is a component of 2nd Piola–Kirchhoff stress. Since the stress is a function of the elastic trial strain and the intermediate configuration is held fixed in the elastic trial process, all the material tensors are referred to the intermediate configuration and thus the linearization is carried out with respect to the intermediate configuration. By considering the return-mapping algorithm in the stress calculation, the consistent tangent operator in the principal stress space can be obtained by

$$\boldsymbol{c}^{\mathrm{alg}} \equiv \frac{\partial \boldsymbol{\tau}^{\mathrm{p}}}{\partial \boldsymbol{e}^{\mathrm{tr}}} = \boldsymbol{c}^{\mathrm{e}} - 4\mu^2 A \boldsymbol{N}\otimes\boldsymbol{N} - \frac{4\mu^2\gamma}{\|\boldsymbol{\eta}^{\mathrm{tr}}\|}(\boldsymbol{I}_{\mathrm{dev}} - \boldsymbol{N}\otimes\boldsymbol{N}) \tag{19}$$

which is $3\times 3$ symmetric matrix in the principal stress space. Eq. (19) has the same form as the classical plasticity except that the principal stress and logarithmic stretch is used here. Using the property in Eq. (18), the stress in Eq. (16) is differentiated to yield

$$\boldsymbol{c} = \frac{\partial \boldsymbol{\tau}}{\partial \boldsymbol{\varepsilon}} = \sum_{i=1}^{3}\sum_{j=1}^{3} c_{ij}^{\mathrm{alg}} \boldsymbol{m}^i\otimes\boldsymbol{m}^j + 2\sum_{i=1}^{3}\tau_i^{\mathrm{p}}\hat{\boldsymbol{c}}^i \tag{20}$$

which contains all the symmetric properties between indices. In Eq. (20), $\hat{\boldsymbol{c}}^i$ is the linearization of $\boldsymbol{m}^i$, which is independent of the plastic flow because the plastic evolution is carried out in the fixed principal direction. The expression of $\hat{\boldsymbol{c}}^i$ is given in detail by Simo and Taylor [33].

### 2.4. Variational principles for finite deformation

Let $\boldsymbol{f}^{\mathrm{B}}$ and $\boldsymbol{f}^{\mathrm{S}}$ be the body force in $\Omega$ and surface traction on $\Gamma_{\mathrm{T}}$. The variational equation at time $t_n$ can be written in different forms depending on the reference configuration used and the stress/strain measures as

$$\begin{aligned} a_\Omega({}^n\boldsymbol{z},\bar{\boldsymbol{z}}) &\equiv \int_\Omega \boldsymbol{\tau}:\bar{\boldsymbol{\varepsilon}}\,\mathrm{d}\Omega = \int_\Omega \boldsymbol{S}:\overline{\boldsymbol{E}}\,\mathrm{d}\Omega \\ &= \int_\Omega \bar{\boldsymbol{z}}^{\mathrm{T}}\boldsymbol{f}^{\mathrm{B}}\,\mathrm{d}\Omega + \int_{\Gamma_{\mathrm{T}}} \bar{\boldsymbol{z}}^{\mathrm{T}}\boldsymbol{f}^{\mathrm{S}}\,\mathrm{d}\Gamma \\ &\equiv \ell_\Omega(\bar{\boldsymbol{z}}), \quad \forall\bar{\boldsymbol{z}}\in Z \end{aligned} \tag{21}$$

where $Z$ is the space of the kinematically admissible displacement. In Eq. (21), overbar "$-$" denotes the first order variation and ":" is the contraction of tensors (i.e., $\boldsymbol{a}:\boldsymbol{b} = a_{ij}b_{ij}$). The notations $a_\Omega({}^n\boldsymbol{z},\bar{\boldsymbol{z}})$ and $\ell_\Omega(\bar{\boldsymbol{z}})$ are used for the structural energy and load linear forms. The left superscript $n$ denotes the configuration time $t_n$ but will be ignored, unless necessary for clarification. The following relations can be obtained from the definition of the stress and strain tensors

$$\boldsymbol{\tau} = \boldsymbol{F}\boldsymbol{S}\boldsymbol{F}^{\mathrm{T}} \tag{22}$$

$$\bar{\boldsymbol{\varepsilon}} = \boldsymbol{F}^{-\mathrm{T}}\overline{\boldsymbol{E}}\boldsymbol{F}^{-1} \tag{23}$$

Using the relations in Eqs. (22) and (23), the updated Lagrangian formulation can be derived from the total Lagrangian formulation. In this way, the equivalence of two formulations can be shown and the basis of DSA can be established. From the definition of the Lagrangian strain tensor $\boldsymbol{E} = (1/2)(\boldsymbol{F}^{\mathrm{T}}\boldsymbol{F} - \boldsymbol{I})$, its variation and increment can be derived as

$$\overline{\boldsymbol{E}} = \frac{1}{2}(\nabla_0\bar{\boldsymbol{z}}^{\mathrm{T}}\boldsymbol{F} + \boldsymbol{F}^{\mathrm{T}}\nabla_0\bar{\boldsymbol{z}}) \tag{24}$$

$$\Delta\boldsymbol{E} = \frac{1}{2}(\nabla_0\Delta\boldsymbol{z}^{\mathrm{T}}\boldsymbol{F} + \boldsymbol{F}^{\mathrm{T}}\nabla_0\Delta\boldsymbol{z}) \tag{25}$$

where the notations $\nabla_0\bar{\boldsymbol{z}} = \partial\bar{\boldsymbol{z}}/\partial\boldsymbol{X}$ and $\nabla_n\bar{\boldsymbol{z}} = \partial\bar{\boldsymbol{z}}/\partial\boldsymbol{x}$ are used henceforth. Since the strain variation in Eq. (24) depends on the displacement, its increment is

$$\Delta\overline{\boldsymbol{E}} = \frac{1}{2}(\nabla_0\bar{\boldsymbol{z}}^{\mathrm{T}}\nabla_0\Delta\boldsymbol{z} + \nabla_0\Delta\boldsymbol{z}^{\mathrm{T}}\nabla_0\bar{\boldsymbol{z}}) \tag{26}$$

Using Eqs. (24)–(26) and $\Delta\boldsymbol{S} = \boldsymbol{C}:\Delta\boldsymbol{E}$, the increment of the integrand of the structural energy form in Eq. (21) is obtained as

$$\Delta(\boldsymbol{S}:\overline{\boldsymbol{E}}) = \overline{\boldsymbol{E}}:\boldsymbol{C}:\Delta\boldsymbol{E} + \boldsymbol{S}:\Delta\overline{\boldsymbol{E}} \tag{27}$$

Thus, the incremental equation of the total Lagrangian formulation becomes

$$\begin{aligned} a_\Omega^*(\boldsymbol{z};\Delta\boldsymbol{z},\bar{\boldsymbol{z}}) &\equiv \int_\Omega (\overline{\boldsymbol{E}}:\boldsymbol{C}:\Delta\boldsymbol{E} + \boldsymbol{S}:\Delta\overline{\boldsymbol{E}})\,\mathrm{d}\Omega \\ &= \ell_\Omega(\bar{\boldsymbol{z}}) - \int_\Omega \boldsymbol{S}:\overline{\boldsymbol{E}}\,\mathrm{d}\Omega \\ &= \ell_\Omega(\bar{\boldsymbol{z}}) - a_\Omega(\boldsymbol{z},\bar{\boldsymbol{z}}), \quad \forall\bar{\boldsymbol{z}}\in Z \end{aligned} \tag{28}$$

To derive the spatial formulation, Eq. (28) is transformed into the current configuration using the relations in Eqs. (22) and (23). That is, each integrand of Eq. (28) can be transformed to the current configuration by

$$\overline{\boldsymbol{E}}:\boldsymbol{C}:\Delta\boldsymbol{E} = \bar{\boldsymbol{\varepsilon}}:\boldsymbol{c}:\boldsymbol{\varepsilon}(\Delta\boldsymbol{z}) \tag{29}$$

$$\boldsymbol{S}:\Delta\overline{\boldsymbol{E}} = \boldsymbol{F}\boldsymbol{S}\boldsymbol{F}^{\mathrm{T}}:(\nabla_n\bar{\boldsymbol{z}}^{\mathrm{T}}\nabla_n\Delta\boldsymbol{z}) = \boldsymbol{\tau}:\boldsymbol{\eta}(\Delta\boldsymbol{z},\bar{\boldsymbol{z}}) \tag{30}$$

where $\boldsymbol{\eta}(\Delta\boldsymbol{z},\bar{\boldsymbol{z}}) = (1/2)(\nabla_n\bar{\boldsymbol{z}}^{\mathrm{T}}\nabla_n\Delta\boldsymbol{z} + \nabla_n\Delta\boldsymbol{z}^{\mathrm{T}}\nabla_n\bar{\boldsymbol{z}})$ is the nonlinear strain increment. Thus, all the necessary terms are transformed to the current configuration. The lin-

earized incremental equation with respect to the current configuration is then

$$a^*_\Omega(\boldsymbol{z};\Delta\boldsymbol{z},\bar{\boldsymbol{z}}) \equiv \int_\Omega [\bar{\boldsymbol{\varepsilon}} : \boldsymbol{c} : \boldsymbol{\varepsilon}(\Delta\boldsymbol{z}) + \boldsymbol{\tau} : \boldsymbol{\eta}(\Delta\boldsymbol{z},\bar{\boldsymbol{z}})]\,\mathrm{d}\Omega = \ell_\Omega(\bar{\boldsymbol{z}}) - a_\Omega(\boldsymbol{z},\bar{\boldsymbol{z}}), \quad \forall \bar{\boldsymbol{z}} \in \mathrm{Z} \tag{31}$$

which is the updated Lagrangian form. Note that Eqs. (28) and (31) are of equivalent formulations and they have the same stiffness matrix and residual. Let the current time be $t_n$ and the iteration count be $k+1$, then the linearization of Eq. (31) using the incremental form becomes

$$a^*_\Omega({}^n\boldsymbol{z}^k;\Delta\boldsymbol{z}^{k+1},\bar{\boldsymbol{z}}) = \int_\Omega [\bar{\boldsymbol{\varepsilon}} : \boldsymbol{c} : \boldsymbol{\varepsilon}(\Delta\boldsymbol{z}^{k+1}) + {}^n\boldsymbol{\tau}^k : \boldsymbol{\eta}(\Delta\boldsymbol{z}^{k+1},\bar{\boldsymbol{z}})]\,\mathrm{d}\Omega = \ell_\Omega(\bar{\boldsymbol{z}}) - a_\Omega({}^n\boldsymbol{z}^k,\bar{\boldsymbol{z}}), \quad \forall \bar{\boldsymbol{z}} \in \mathrm{Z} \tag{32}$$

Eq. (32) is solved iteratively until the right side, which is the residual force, vanishes. After convergence, time step is advanced and the same procedure repeats until the final configuration is reached. Notice that the integration of the internal energy term is carried out in the undeformed configuration because of the employment of the Kirchhoff stress. Even if two formulations are equivalent, the choice of the specific formulation depends crucially upon the constitutive relation.

## 3. Shape design sensitivity formulation for finite elastoplasticity: spatial description

In shape DSA of the nonlinear elastic material, even if analysis is carried out incrementally, it is well known that the sensitivity equation is linear and needs to be solved only one time at the final converged configuration with tangent stiffness matrix the same as that of the incremental analysis. Two types of formulations are usually used in the literature: the total Lagrangian and updated Lagrangian formulations. The first one uses the undeformed configuration as a reference and in the second case current configuration is the reference, and these two methods are mathematically equivalent. However, from the sensitivity point of view, the equivalence of the two formulations is not established clearly. Since the perturbation of the design is defined only on the initial (undeformed) configuration, the total Lagrangian formulation is a more natural choice [35]. Cho and Choi [13] discussed updating design velocity fields for each time step by incorporating shape DSA with respect to the updated Lagrangian formulation for the elastoplastic material. The design velocity fields at the current time are computed using the displacement sensitivity and the design velocity at the previous time. Thus, the sensitivity equation has to be solved at each time step for the material model that is elastic or hyperelastic for updated Lagrangian formulation. This procedure is very inefficient compared to the total Lagrangian formulation. However, in the updated Lagrangian formulation of the sizing DSA done by Choi and Santos [34], the sensitivity equation is solved only once at the final converged time step. In this section, a shape DSA of the updated Lagrangian formulation that needs to be solved only once that the final converged configuration is proposed for elastic or hyperelastic material.

### 3.1. Material derivatives

In shape DSA, the shape of the domain that a structural component occupies is treated as the design variable. Consider an undeformed domain $\Omega$ with boundary $\Gamma$ at the initial design $\tau = 0$ as shown in Fig. 1. Suppose that only one parameter $\tau$ defines the mapping $\boldsymbol{T}$ for shape perturbation between original geometry and perturbed geometry. The mapping for shape perturbation $\boldsymbol{T} : \boldsymbol{X} \to \boldsymbol{X}_\tau(\boldsymbol{X})$, $\boldsymbol{X} \in \Omega$, is given by

$$\begin{aligned} \boldsymbol{X}_\tau &= \boldsymbol{T}(\boldsymbol{X},\tau) \\ \Omega_\tau &= \boldsymbol{T}(\Omega,\tau) \\ \Gamma_\tau &= \boldsymbol{T}(\Gamma,\tau) \end{aligned} \tag{33}$$

The mapping of Eq. (33) can be interpreted as a dynamic process perturbing a continuum shape design from an initial domain $\Omega$, at $\tau = 0$, to a perturbed domain $\Omega_\tau$. Define a design velocity field as

$$\boldsymbol{V}(\boldsymbol{X}_\tau,\tau) \equiv \frac{\mathrm{d}\boldsymbol{X}_\tau}{\mathrm{d}\tau} = \frac{\mathrm{d}\boldsymbol{T}(\boldsymbol{X},\tau)}{\mathrm{d}\tau} = \frac{\partial \boldsymbol{T}(\boldsymbol{X},\tau)}{\partial\tau} \tag{34}$$

with $\tau$ playing the role of time. In a neighborhood of $\tau = 0$, under the reasonable regularity hypothesis and ignoring higher order terms,

$$\boldsymbol{T}(\boldsymbol{X},\tau) = \boldsymbol{T}(\boldsymbol{X},0) + \tau\frac{\mathrm{d}\boldsymbol{T}(\boldsymbol{X},0)}{\mathrm{d}\tau} + \mathrm{O}(\tau^2) \approx \boldsymbol{X} + \tau\boldsymbol{V}(\boldsymbol{X},0) \tag{35}$$

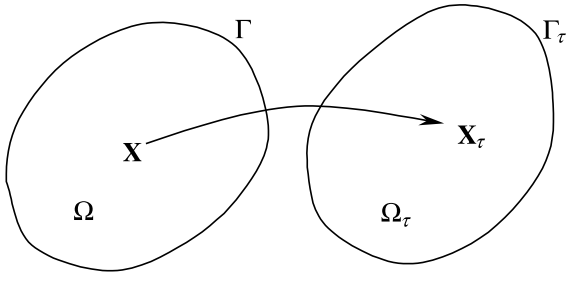


Fig. 1. Variation of undeformed domain by one-parameter family of mappings.

where $\boldsymbol{X} \equiv \boldsymbol{T}(\boldsymbol{X},0)$ and $\boldsymbol{V}(\boldsymbol{X}) \equiv \boldsymbol{V}(\boldsymbol{X},0)$ Detailed formula for material derivative can be found in Ref. [1]. The material derivative of the domain integral functional

$$\Psi_\tau = \int_{\Omega_\tau} g_\tau(\boldsymbol{X}_\tau)\mathrm{d}\Omega \tag{36}$$

is

$$\frac{\mathrm{d}}{\mathrm{d}\tau}(\Psi_\tau)\bigg|_{\tau=0} = \int_\Omega [\dot{g}(\boldsymbol{X}) + g(\boldsymbol{X})\mathrm{div}\,\boldsymbol{V}]\mathrm{d}\Omega \tag{37}$$

where $\dot{g} \equiv \mathrm{d}g/\mathrm{d}\tau$. The material derivative of the boundary integral functional

$$\Psi_\tau = \int_{\Gamma_\tau} g_\tau(\boldsymbol{X}_\tau)\mathrm{d}\Gamma \tag{38}$$

is

$$\frac{\mathrm{d}}{\mathrm{d}\tau}(\Psi_\tau)\bigg|_{\tau=0} = \int_\Gamma [\dot{g}(\boldsymbol{X}) + \kappa g(\boldsymbol{X})V_\mathrm{n}]\mathrm{d}\Gamma \tag{39}$$

where $\kappa$ is the curvature of the boundary and $V_\mathrm{n}$ is the normal component of the design velocity. Eq. (37) can be used to obtain derivatives of the structural variational form and the performance measure that is defined as a domain integral. Eq. (39) can be used obtaining the derivatives of the performance measure that is defined as a boundary integral.

The solution $\boldsymbol{z}_\tau(\boldsymbol{X}_\tau)$ of Eq. (21) referring to the initial coordinates $\boldsymbol{X}_\tau$ of the perturbed domain is assumed to be a differentiable function with respect to the shape design variable. The mapping $\boldsymbol{z}_\tau(\boldsymbol{X}_\tau) \equiv \boldsymbol{z}_\tau(\boldsymbol{X} + \tau\boldsymbol{V}(\boldsymbol{X}))$ is defined on $\Omega$, and $\boldsymbol{z}_\tau(\boldsymbol{X}_\tau)$ depends on $\tau$ in two ways. First, it is the solution to the equilibrium of Eq. (21) on $\Omega_\tau$. Second, it is evaluated at a point $\boldsymbol{X}_\tau$ that moves with $\tau$. The pointwise material derivative of $\boldsymbol{z}_\tau(\boldsymbol{X}_\tau)$ at $\boldsymbol{X} \in \Omega$, if it exists, is defined as

$$\begin{aligned}\dot{\boldsymbol{z}} &\equiv \frac{\mathrm{d}}{\mathrm{d}\tau}\boldsymbol{z}_\tau(\boldsymbol{X} + \tau\boldsymbol{V}(\boldsymbol{X}))|_{\tau=0} \\ &= \lim_{\tau\to 0}\frac{\boldsymbol{z}_\tau(\boldsymbol{X} + \tau\boldsymbol{V}(\boldsymbol{X})) - \boldsymbol{z}(\boldsymbol{X})}{\tau}\end{aligned} \tag{40}$$

If $\boldsymbol{z}_\tau(\boldsymbol{X}_\tau)$ has a regular extension to a neighborhood of $\overline{\Omega}_\tau$, then

$$\dot{\boldsymbol{z}}(\boldsymbol{X}) = \boldsymbol{z}'(\boldsymbol{X}) + \nabla_0\boldsymbol{z}\boldsymbol{V}(\boldsymbol{X}) \tag{41}$$

where

$$\boldsymbol{z}' \equiv \lim_{\tau\to 0}\frac{\boldsymbol{z}_\tau(\boldsymbol{X}) - \boldsymbol{z}(\boldsymbol{X})}{\tau} \tag{42}$$

is the partial derivative of $\boldsymbol{z}_\tau$ and $\nabla_0\boldsymbol{z} \equiv [\nabla_0 z_1, \nabla_0 z_2, \nabla_0 z_3]^\mathrm{T}$.

### 3.2. Shape design sensitivity analysis of finite elasticity

In this section, a new shape design sensitivity formulation for the updated Lagrangian formulation with the same efficiency as the total Lagrangian formulation is proposed for the elastic material. The design derivative is taken at the undeformed configuration, and then all the variables are transformed to the current configuration using a similar procedure as the one described in Eq. (31). Since, the sensitivity equation at the current configuration is the transformation from the undeformed configuration, two formulations give the same fictitious load form but different representations.

After computing all necessary terms of DSA using the total Lagrangian description, these terms will be transformed to the current configuration to be consistent with response analysis. This approach is important because the shape design is perturbed at the undeformed configuration. The design derivative of structural energy form becomes

$$\frac{\mathrm{d}}{\mathrm{d}\tau}\int_{\Omega_\tau}\boldsymbol{S}:\overline{\boldsymbol{E}}\,\mathrm{d}\Omega = \int_\Omega(\dot{\boldsymbol{S}}:\overline{\boldsymbol{E}} + \boldsymbol{S}:\dot{\overline{\boldsymbol{E}}} + \boldsymbol{S}:\overline{\boldsymbol{E}}\,\mathrm{div}\,\boldsymbol{V})\,\mathrm{d}\Omega \tag{43}$$

where $\mathrm{d}/\mathrm{d}\tau(\cdot)$ denotes the design derivative, whereas $\mathrm{d}/\mathrm{d}t(\cdot)$ represents the time derivative in the response analysis. In Eq. (43), $\boldsymbol{V}$ denotes the design velocity field, which represents the direction and the magnitude of the shape perturbation at the undeformed geometry. The last term $\mathrm{div}\,\boldsymbol{V}$ comes from the domain perturbation effect. The first part on the right of Eq. (43) can be expressed in terms of the displacement sensitivity and design velocity by using the constitutive relation.

The material derivative of the stress can be expressed in terms of the material derivative of the strain as

$$\dot{\boldsymbol{S}} = \boldsymbol{C}:\dot{\boldsymbol{E}} \tag{44}$$

where $\boldsymbol{C}$ is fourth order material constitutive tensor defined in Eq. (18). Since the Lagrangian strain tensor is defined in terms of the deformation gradient, the design derivative of $\boldsymbol{F}$ is obtained as

$$\dot{\boldsymbol{F}} = \frac{\mathrm{d}}{\mathrm{d}\tau}(\boldsymbol{I} + \nabla_0\boldsymbol{z}) = \nabla_0\dot{\boldsymbol{z}} - \nabla_0\boldsymbol{z}\nabla_0\boldsymbol{V} \tag{45}$$

where $\dot{\boldsymbol{z}} = \mathrm{d}/\mathrm{d}\tau(\boldsymbol{z})$ is the material derivative of the displacement vector. In Eq. (45), the property that the partial derivative with respect to design can be exchanged with the spatial gradient at the reference configuration is used [1]. Thus, the material derivative of the Lagrangian strain tensor can be expressed as

$$\dot{\boldsymbol{E}} = \frac{1}{2}[(\nabla_0\dot{\boldsymbol{z}} - \nabla_0\boldsymbol{z}\nabla_0\boldsymbol{V})^\mathrm{T}\boldsymbol{F} + \boldsymbol{F}^\mathrm{T}(\nabla_0\dot{\boldsymbol{z}} - \nabla_0\boldsymbol{z}\nabla_0\boldsymbol{V})] \tag{46}$$

By using the property in Eq. (23), Eq. (46) can be transformed into the current configuration as

$$\boldsymbol{F}^{-\mathrm{T}}\dot{\boldsymbol{E}}\boldsymbol{F}^{-1} \equiv \boldsymbol{\varepsilon}(\dot{\boldsymbol{z}}) + \boldsymbol{\varepsilon}_{\mathrm{V}}(\boldsymbol{z}) \tag{47}$$

where

$$\boldsymbol{\varepsilon}_{\mathrm{V}}(\boldsymbol{z}) = -\frac{1}{2}\left(\nabla_0 \boldsymbol{z}\nabla_n \boldsymbol{V} + \nabla_n \boldsymbol{V}^{\mathrm{T}}\nabla_0 \boldsymbol{z}^{\mathrm{T}}\right) \tag{48}$$

denotes the explicit dependence on the design velocity field and response. Note that $\boldsymbol{\varepsilon}_{\mathrm{V}}(\boldsymbol{z})$ contains two different gradient operators, $\nabla_0$ and $\nabla_n$. Thus, the spatial description of the first integrand on the right of Eq. (43) can be expressed as

$$\dot{\boldsymbol{S}} : \overline{\boldsymbol{E}} = \overline{\boldsymbol{E}} : \boldsymbol{C} : \dot{\boldsymbol{E}} = \bar{\boldsymbol{\varepsilon}} : \boldsymbol{c} : \boldsymbol{\varepsilon}(\dot{\boldsymbol{z}}) + \bar{\boldsymbol{\varepsilon}} : \boldsymbol{c} : \boldsymbol{\varepsilon}_{\mathrm{V}}(\boldsymbol{z}) \tag{49}$$

Eq. (49) separates the stress sensitivity into known and unknown parts. The known part $\bar{\boldsymbol{\varepsilon}} : \boldsymbol{c} : \boldsymbol{\varepsilon}_{\mathrm{V}}(\boldsymbol{z})$ can be computed using the design velocity and current response. The unknown part $\bar{\boldsymbol{\varepsilon}} : \boldsymbol{c} : \boldsymbol{\varepsilon}(\dot{\boldsymbol{z}})$ yields $a^*_{\Omega}(\boldsymbol{z}; \dot{\boldsymbol{z}}, \bar{\boldsymbol{z}})$ when $\Delta\boldsymbol{z}$ is replaced by $\dot{\boldsymbol{z}}$.

For the second part of Eq. (43), the material derivative of the strain variation is obtained, using Eqs. (24) and (45),

$$\begin{aligned}\dot{\bar{\boldsymbol{E}}} &= \frac{\mathrm{d}}{\mathrm{d}\tau}\frac{1}{2}(\nabla_0 \bar{\boldsymbol{z}}^{\mathrm{T}}\boldsymbol{F} + \boldsymbol{F}^{\mathrm{T}}\nabla_0 \bar{\boldsymbol{z}}) \\ &= -\frac{1}{2}[(\nabla_0 \bar{\boldsymbol{z}}\nabla_0 \boldsymbol{V})^{\mathrm{T}}\boldsymbol{F} + \boldsymbol{F}^{\mathrm{T}}(\nabla_0 \bar{\boldsymbol{z}}\nabla_0 \boldsymbol{V})] + \frac{1}{2}[\nabla_0 \bar{\boldsymbol{z}}^{\mathrm{T}}(\nabla_0 \dot{\boldsymbol{z}} \\ &\quad - \nabla_0 \boldsymbol{z}\nabla_0 \boldsymbol{V}) + (\nabla_0 \dot{\boldsymbol{z}} - \nabla_0 \boldsymbol{z}\nabla_0 \boldsymbol{V})^{\mathrm{T}}\nabla_0 \bar{\boldsymbol{z}}]\end{aligned} \tag{50}$$

By pre-multiplying $\boldsymbol{F}^{-1}$ as in Eq. (47), Eq. (50) becomes

$$\boldsymbol{F}^{-\mathrm{T}}\dot{\bar{\boldsymbol{E}}}\boldsymbol{F}^{-1} \equiv \boldsymbol{\eta}(\dot{\boldsymbol{z}}, \bar{\boldsymbol{z}}) + \boldsymbol{\eta}_{\mathrm{V}}(\boldsymbol{z}, \bar{\boldsymbol{z}}) \tag{51}$$

where

$$\begin{aligned}\boldsymbol{\eta}_{\mathrm{V}}(\boldsymbol{z}, \bar{\boldsymbol{z}}) = &-\frac{1}{2}[\nabla_n \bar{\boldsymbol{z}}^{\mathrm{T}}(\nabla_0 \boldsymbol{z}\nabla_n \boldsymbol{V}) + (\nabla_0 \boldsymbol{z}\nabla_n \boldsymbol{V})^{\mathrm{T}}\nabla_n \bar{\boldsymbol{z}}] \\ &-\frac{1}{2}[(\nabla_0 \bar{\boldsymbol{z}}\nabla_n \boldsymbol{V}) + (\nabla_0 \bar{\boldsymbol{z}}\nabla_n \boldsymbol{V})^{\mathrm{T}}]\end{aligned} \tag{52}$$

Thus, the second integrand on the right of Eq. (43) can be expressed in terms of the current configuration as

$$\boldsymbol{S} : \dot{\bar{\boldsymbol{E}}} = \boldsymbol{\tau} : \boldsymbol{\eta}(\dot{\boldsymbol{z}}, \bar{\boldsymbol{z}}) + \boldsymbol{\tau} : \boldsymbol{\eta}_{\mathrm{V}}(\boldsymbol{z}, \bar{\boldsymbol{z}}) \tag{53}$$

By substituting Eqs. (49) and (53) into Eq. (43), the material derivative of the structural energy form at the current configuration can be obtained as

$$\frac{\mathrm{d}}{\mathrm{d}\tau}[a(\boldsymbol{z}, \bar{\boldsymbol{z}})] \equiv a^*_{\Omega}(\boldsymbol{z}; \dot{\boldsymbol{z}}, \bar{\boldsymbol{z}}) + a'_{\mathrm{V}}(\boldsymbol{z}, \bar{\boldsymbol{z}}) \tag{54}$$

where

$$a'_{\mathrm{V}}(\boldsymbol{z}, \bar{\boldsymbol{z}}) = \int_{\Omega}[\bar{\boldsymbol{\varepsilon}} : \boldsymbol{c} : \boldsymbol{\varepsilon}_{\mathrm{V}}(\boldsymbol{z}) + \boldsymbol{\tau} : \boldsymbol{\eta}_{\mathrm{V}}(\boldsymbol{z}, \bar{\boldsymbol{z}}) + \boldsymbol{\tau} : \bar{\boldsymbol{\varepsilon}}\,\mathrm{div}\,\boldsymbol{V}]\,\mathrm{d}\Omega \tag{55}$$

is the *structural fictitious load form*, which is linear in $\boldsymbol{V}$ and $\boldsymbol{z}$. Once the results of response analysis, $\boldsymbol{z}$ and $\boldsymbol{\tau}$, are given at the current time, $a'_{\mathrm{V}}(\boldsymbol{z}, \bar{\boldsymbol{z}})$ can be computed explicitly without any sensitivity information from the previous configuration. Note that the spatial fictitious load form $a'_{\mathrm{V}}(\boldsymbol{z}, \bar{\boldsymbol{z}})$ in Eq. (55) is a transformed version of the material fictitious load form given by Santos and Choi [35]. These two approaches yield the same fictitious load vectors. Thus, the same design sensitivity result $\dot{\boldsymbol{z}}$ is expected from these two formulations.

The material derivative of the load linear form in Eq. (21) can be obtained as

$$\begin{aligned}\ell'_{\mathrm{V}}(\bar{\boldsymbol{z}}) = &\int_{\Omega}\left[\bar{\boldsymbol{z}}^{\mathrm{T}}(\nabla \boldsymbol{f}^{\mathrm{B}}\boldsymbol{V}) + \bar{\boldsymbol{z}}^{\mathrm{T}}\boldsymbol{f}^{\mathrm{B}}\,\mathrm{div}\,\boldsymbol{V}\right]\mathrm{d}\Omega \\ &+ \int_{\Gamma_{\mathrm{T}}}\left[\bar{\boldsymbol{z}}^{\mathrm{T}}(\nabla \boldsymbol{f}^{\mathrm{S}}\boldsymbol{V}) + \kappa\bar{\boldsymbol{z}}^{\mathrm{T}}\boldsymbol{f}^{\mathrm{S}}V_{\mathrm{n}}\right]\mathrm{d}\Gamma\end{aligned} \tag{56}$$

Here it is assumed that the external force is independent of the design change, i.e., $\boldsymbol{f}^{\mathrm{B}'} = \boldsymbol{f}^{\mathrm{S}'} = 0$. Eq. (56) is defined as the *external fictitious load*. Starting from the undeformed reference frame, after proper transformation, the sensitivity equation corresponding to the current configuration is obtained as

$$a^*_{\Omega}(\boldsymbol{z}; \dot{\boldsymbol{z}}, \bar{\boldsymbol{z}}) = \ell'_{\mathrm{V}}(\bar{\boldsymbol{z}}) - a'_{\mathrm{V}}(\boldsymbol{z}, \bar{\boldsymbol{z}}), \quad \forall \bar{\boldsymbol{z}} \in \mathrm{Z} \tag{57}$$

Note that the sensitivity equation, Eq. (57), is solved only once at the final converged time with the same stiffness matrix as that in the response analysis, and the solution of Eq. (57) is not an incremental sensitivity, but the total displacement sensitivity. To conclude, the sensitivity equation of the updated Lagrangian formulation is equivalent to the sensitivity equation of the total Lagrangian formulation, and the total form of the sensitivity equation can be obtained if the constitutive equation is given as a total form.

### 3.3. Shape design sensitivity formulation for finite deformation elastoplasticity

When the material deformation is in the plastic range, the intermediate configuration contributes to the sensitivity formulation. The reference frame of response analysis, which is the intermediate configuration, is different from the reference frame of design perturbation, which is the undeformed configuration. Fig. 2 shows the procedure for response analysis and design perturbation. The transformation between the undeformed and intermediate configurations is not involved in the linearization of response analysis because it is fixed in the elastic trial process. Since the intermediate configuration is changed as the shape design is perturbed in the undeformed configuration in DSA, this transformation is not fixed from the sensitivity viewpoint. The path-dependency of the sensitivity equation comes from this

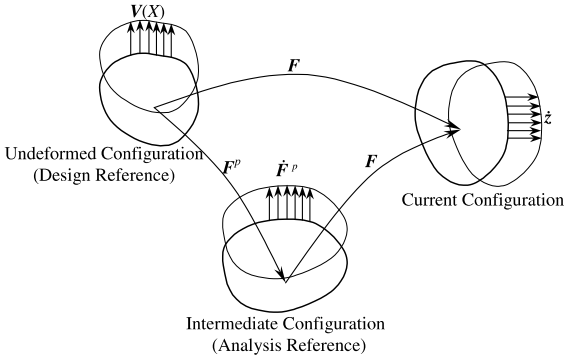


Fig. 2. Illustration of analysis and design perturbation procedure.

transformation as well as the dependency of the plastic evolution variables.

Since response analysis refers to the intermediate configuration, the material derivative of the elastic trial Lagrangian strain tensor $\boldsymbol{E}^{\mathrm{e}} = (1/2)[\boldsymbol{F}^{\mathrm{e}^{\mathrm{T}}}\boldsymbol{F}^{\mathrm{e}} - \boldsymbol{I}]$ in the intermediate configuration is

$$\dot{\boldsymbol{E}}^{\mathrm{e}} = \frac{1}{2}(\dot{\boldsymbol{F}}^{\mathrm{e}^{\mathrm{T}}}\boldsymbol{F}^{\mathrm{e}} + \boldsymbol{F}^{\mathrm{e}^{\mathrm{T}}}\dot{\boldsymbol{F}}^{\mathrm{e}}) \tag{58}$$

and the transformation of Eq. (58) into the current configuration leads to

$$\boldsymbol{F}^{\mathrm{e}^{-\mathrm{T}}}\dot{\boldsymbol{E}}^{\mathrm{e}}\boldsymbol{F}^{\mathrm{e}^{-1}} = \frac{1}{2}(\boldsymbol{F}^{\mathrm{e}^{-\mathrm{T}}}\dot{\boldsymbol{F}}^{\mathrm{e}^{\mathrm{T}}} + \dot{\boldsymbol{F}}^{\mathrm{e}}\boldsymbol{F}^{\mathrm{e}^{-1}}) \tag{59}$$

Note that the push-forward transformation is from the intermediate configuration to the current configuration. Since $\dot{\boldsymbol{F}}^{\mathrm{e}}$ refers to the intermediate configuration, it should be transformed to the undeformed configuration where the design velocity is given explicitly, by taking the material derivative of decomposition in Eq. (1). By using $\dot{\boldsymbol{F}}^{\mathrm{e}} = \dot{\boldsymbol{F}}\boldsymbol{F}^{\mathrm{p}^{-1}} - \boldsymbol{F}^{\mathrm{e}}\dot{\boldsymbol{F}}^{\mathrm{p}}\boldsymbol{F}^{\mathrm{p}^{-1}}$ and defining a path-dependent matrix $\boldsymbol{G}$ as

$$\boldsymbol{G} = \boldsymbol{F}^{\mathrm{e}}\dot{\boldsymbol{F}}^{\mathrm{p}}\boldsymbol{F}^{-1} \tag{60}$$

which is a transformation of $\dot{\boldsymbol{F}}^{\mathrm{p}}$ into the current configuration, Eq. (59) can be rearranged as

$$\begin{aligned}\boldsymbol{F}^{\mathrm{e}^{-\mathrm{T}}}\dot{\boldsymbol{E}}^{\mathrm{e}}\boldsymbol{F}^{\mathrm{e}^{-1}} &= \frac{1}{2}(\boldsymbol{F}^{-\mathrm{T}}\dot{\boldsymbol{F}}^{\mathrm{T}} + \dot{\boldsymbol{F}}\boldsymbol{F}^{-1}) - \frac{1}{2}(\boldsymbol{G} + \boldsymbol{G}^{\mathrm{T}}) \\ &\equiv \boldsymbol{\varepsilon}(\dot{\boldsymbol{z}}) + \boldsymbol{\varepsilon}_{\mathrm{V}}(\boldsymbol{z}) + \boldsymbol{\varepsilon}_{\mathrm{P}}(\boldsymbol{z})\end{aligned} \tag{61}$$

where $\boldsymbol{\varepsilon}(\dot{\boldsymbol{z}})$ and $\boldsymbol{\varepsilon}_{\mathrm{V}}(\boldsymbol{z})$ are the same forms as the sensitivity formulation in the finite elasticity and $\boldsymbol{\varepsilon}_{\mathrm{P}}(\boldsymbol{z})$ is the contribution from the elastic trial intermediate configuration where the path-dependency comes from

$$\boldsymbol{\varepsilon}_{\mathrm{P}}(\boldsymbol{z}) = -\frac{1}{2}(\boldsymbol{G} + \boldsymbol{G}^{\mathrm{T}}) \tag{62}$$

While left side of Eq. (61) is the push forward transformation, the right side of Eq. (61) is equivalent to pulling back $\boldsymbol{E}^{\mathrm{e}}$ to the undeformed configuration, taking the material derivative, and pushing forward to the current configuration. The trial elastic deformation gradient $\boldsymbol{F}^{\mathrm{e}}$ must be extracted from response analysis and the material derivative of $\boldsymbol{F}^{\mathrm{p}}$ must be stored from the previous sensitivity procedure. An interesting observation can be made from the comparison of the rate form and multiplicative plasticity: (1) in additive rateform plasticity, the path-dependency is resulting from the design derivative of the stress tensor at the previous time step and, (2) in multiplicative plasticity, the path-dependency is due to the transformation between the intermediate and current configurations.

The same procedure must be applied to the variation of the Lagrangian strain tensor $\overline{\boldsymbol{E}}^{\mathrm{e}} = (1/2)[\overline{\boldsymbol{F}}^{\mathrm{e}^{\mathrm{T}}}\boldsymbol{F}^{\mathrm{e}} + \boldsymbol{F}^{\mathrm{e}^{\mathrm{T}}}\overline{\boldsymbol{F}}^{\mathrm{e}}]$ in the intermediate configuration as

$$\boldsymbol{F}^{\mathrm{e}^{-\mathrm{T}}}\dot{\overline{\boldsymbol{E}}}^{\mathrm{e}}\boldsymbol{F}^{\mathrm{e}^{-1}} \equiv \boldsymbol{\eta}(\dot{\boldsymbol{z}}, \overline{\boldsymbol{z}}) + \boldsymbol{\eta}_{\mathrm{V}}(\boldsymbol{z}, \overline{\boldsymbol{z}}) + \boldsymbol{\eta}_{\mathrm{P}}(\boldsymbol{z}, \overline{\boldsymbol{z}}) \tag{63}$$

where, $\boldsymbol{\eta}_{\mathrm{P}}(\boldsymbol{z}, \overline{\boldsymbol{z}})$ is obtained using a similar procedure as for $\boldsymbol{\varepsilon}_{\mathrm{P}}(\boldsymbol{z})$,

$$\boldsymbol{\eta}_{\mathrm{P}}(\boldsymbol{z}, \overline{\boldsymbol{z}}) = -\frac{1}{2}(\nabla_n\overline{\boldsymbol{z}}\boldsymbol{G} + \nabla_n\overline{\boldsymbol{z}}^{\mathrm{T}}\boldsymbol{G} + \boldsymbol{G}^{\mathrm{T}}\nabla_n\overline{\boldsymbol{z}} + \boldsymbol{G}^{\mathrm{T}}\nabla_n\overline{\boldsymbol{z}}^{\mathrm{T}}) \tag{64}$$

which is the contribution of the elastic trial intermediate configuration through the nonlinear strain term.

The material derivative of the Kirchhoff stress in Eq. (16) becomes

$$\dot{\boldsymbol{\tau}} = \sum_{i=1}^{3}(\dot{\tau}_i^{\mathrm{p}}\boldsymbol{m}^i + \tau_i^{\mathrm{p}}\dot{\boldsymbol{m}}^i) \tag{65}$$

The material derivative of the principal stress is a function of the principal logarithmic strain. The following relation can be obtained by the chain rule of differentiation and the push-forward operation,

$$\begin{aligned}\dot{\tau}_i^{\mathrm{p}} &= \sum_{j=1}^{3}\frac{\partial\tau_i^{\mathrm{p}}}{\partial e_j^{\mathrm{tr}}}\left(2\boldsymbol{F}^{\mathrm{e}}\frac{\partial e_j^{\mathrm{tr}}}{\partial\boldsymbol{C}^{\mathrm{e}}}\boldsymbol{F}^{\mathrm{e}^{\mathrm{T}}}\right) : (\boldsymbol{F}^{\mathrm{e}^{-\mathrm{T}}}\dot{\boldsymbol{E}}^{\mathrm{e}}\boldsymbol{F}^{\mathrm{e}^{-1}}) + \frac{\partial\tau_i^{\mathrm{p}}}{\partial e^{\mathrm{p}}}\dot{e}_n^{\mathrm{p}} + \frac{\partial\tau_i^{\mathrm{p}}}{\partial\boldsymbol{\alpha}}\dot{\boldsymbol{\alpha}}_n \\ &= \sum_{j=1}^{3}c_{ij}^{\mathrm{alg}}\boldsymbol{m}^j : [\boldsymbol{\varepsilon}(\dot{\boldsymbol{z}}) + \boldsymbol{\varepsilon}_{\mathrm{V}}(\boldsymbol{z}) + \boldsymbol{\varepsilon}_{\mathrm{P}}(\boldsymbol{z})] + \frac{\partial\tau_i^{\mathrm{p}}}{\partial e^{\mathrm{p}}}\dot{e}_n^{\mathrm{p}} + \frac{\partial\tau_i^{\mathrm{p}}}{\partial\boldsymbol{\alpha}}\dot{\boldsymbol{\alpha}}_n\end{aligned} \tag{66}$$

where

$$\frac{\partial\boldsymbol{\tau}^{\mathrm{p}}}{\partial\boldsymbol{\alpha}} = 2\mu A\boldsymbol{N}\otimes\boldsymbol{N} + \frac{2\mu\gamma}{\|\boldsymbol{\eta}^{\mathrm{tr}}\|}(\boldsymbol{I}_{\mathrm{dev}} - \boldsymbol{N}\otimes\boldsymbol{N}) \tag{67}$$

$$\frac{\partial\boldsymbol{\tau}^{\mathrm{p}}}{\partial e^{\mathrm{p}}} = 2\mu A\kappa'\boldsymbol{N} \tag{68}$$

are of the same forms as those in the sensitivity formulation for the classical infinitesimal plasticity. The path-dependency of the material derivative of the Kirchhoff stress comes from $\boldsymbol{\varepsilon}_{\mathrm{P}}(\boldsymbol{z})$, $\boldsymbol{\eta}_{\mathrm{P}}(\boldsymbol{z}, \overline{\boldsymbol{z}})$, $\dot{\boldsymbol{\alpha}}_n$, and $\dot{e}_n^{\mathrm{p}}$. Since $\boldsymbol{m}^i$ is only related to the elastic trial state, it is independent of

the plastic evolution and its material derivative can be obtained from the derivative of the elastic trial strain:

$$\dot{\boldsymbol{m}}^i = \left(2\boldsymbol{F}^{\mathrm{e}}\frac{\partial \boldsymbol{m}^i}{\partial \boldsymbol{C}^{\mathrm{e}}}\boldsymbol{F}^{\mathrm{e}^{\mathrm{T}}}\right) : (\boldsymbol{F}^{\mathrm{e}^{-\mathrm{T}}}\dot{\boldsymbol{E}}^{\mathrm{e}}\boldsymbol{F}^{\mathrm{e}^{-1}}) = 2\hat{\boldsymbol{c}}^i : [\boldsymbol{\varepsilon}(\dot{\boldsymbol{z}}) + \boldsymbol{\varepsilon}_{\mathrm{V}}(\boldsymbol{z}) + \boldsymbol{\varepsilon}_{\mathrm{P}}(\boldsymbol{z})] \tag{69}$$

Thus, the design derivative of the Kirchhoff stress tensor can be expressed in terms of $\dot{\boldsymbol{z}}$, configuration of response analysis, and sensitivity results of the previous time step, as

$$\begin{aligned}\dot{\boldsymbol{\tau}} &= \sum_{i=1}^{3}(\dot{\tau}_i^{\mathrm{p}}\boldsymbol{m}^i + \tau_i^{\mathrm{p}}\dot{\boldsymbol{m}}^i)\\ &= \sum_{i=1}^{3}\sum_{j=1}^{3}(c_{ij}^{\mathrm{alg}}\boldsymbol{m}^i\otimes\boldsymbol{m}^j + 2\tau_i^{\mathrm{p}}\hat{\boldsymbol{c}}^i) : [\boldsymbol{\varepsilon}(\dot{\boldsymbol{z}}) + \boldsymbol{\varepsilon}_{\mathrm{V}}(\boldsymbol{z}) + \boldsymbol{\varepsilon}_{\mathrm{P}}(\boldsymbol{z})] + \boldsymbol{\tau}^{\mathrm{fic}}\\ &= \boldsymbol{c} : [\boldsymbol{\varepsilon}(\dot{\boldsymbol{z}}) + \boldsymbol{\varepsilon}_{\mathrm{V}}(\boldsymbol{z}) + \boldsymbol{\varepsilon}_{\mathrm{P}}(\boldsymbol{z})] + \boldsymbol{\tau}^{\mathrm{fic}}\end{aligned} \tag{70}$$

where $\boldsymbol{c}$ is the fourth order consistent tangent stiffness tensor at the current configuration and

$$\boldsymbol{\tau}^{\mathrm{fic}} = \sum_{i=1}^{3}\left(\frac{\partial\tau_i^{\mathrm{p}}}{\partial\boldsymbol{\alpha}}\dot{\boldsymbol{\alpha}}_n + \frac{\partial\tau_i^{\mathrm{p}}}{\partial e^{\mathrm{p}}}\dot{e}_n^{\mathrm{p}}\right)\boldsymbol{m}^i \tag{71}$$

is the path-dependent term due to plastic evolution. The $\boldsymbol{\tau}^{\mathrm{fic}}$ term must be included when the material is in the plastic range. It is clear from Eq. (71) that the sensitivity information of $\dot{\boldsymbol{\alpha}}_n$ and $\dot{e}_n^{\mathrm{p}}$ at the previous time step needs to be stored for the displacement sensitivity computation at the current time step.

From the material derivative of the Kirchhoff stress in Eq. (70) and the transformation of the material derivatives of the Lagrangian strain tensor to the current configuration in Eqs. (61) and (63), the material derivative of the structural variational form can be obtained as

$$\frac{\mathrm{d}}{\mathrm{d}\tau}[a(\boldsymbol{z},\bar{\boldsymbol{z}})] = \frac{\mathrm{d}}{\mathrm{d}\tau}\int_{\Omega}\boldsymbol{\tau} : \bar{\boldsymbol{\varepsilon}}\,\mathrm{d}\Omega \equiv a^*(\boldsymbol{z};\dot{\boldsymbol{z}},\bar{\boldsymbol{z}}) + a'_{\mathrm{V}}(\boldsymbol{z},\bar{\boldsymbol{z}}) \tag{72}$$

where

$$\begin{aligned}a'_{\mathrm{V}}(\boldsymbol{z},\bar{\boldsymbol{z}}) = &\int_{\Omega}[\bar{\boldsymbol{\varepsilon}} : \boldsymbol{c} : \boldsymbol{\varepsilon}_{\mathrm{V}}(\boldsymbol{z}) + \boldsymbol{\tau} : \boldsymbol{\eta}_{\mathrm{V}}(\boldsymbol{z},\bar{\boldsymbol{z}}) + \boldsymbol{\tau} : \bar{\boldsymbol{\varepsilon}}\,\mathrm{div}\,\boldsymbol{V}]\,\mathrm{d}\Omega\\ &+ \int_{\Omega}[\bar{\boldsymbol{\varepsilon}} : \boldsymbol{c} : \boldsymbol{\varepsilon}_{\mathrm{P}}(\boldsymbol{z}) + \boldsymbol{\tau} : \boldsymbol{\eta}_{\mathrm{P}}(\boldsymbol{z},\bar{\boldsymbol{z}}) + \boldsymbol{\tau}^{\mathrm{fic}} : \bar{\boldsymbol{\varepsilon}}]\,\mathrm{d}\Omega\end{aligned} \tag{73}$$

is the *structural fictitious load form* for the finite plasticity that can be computed from the result of response analysis and the result of sensitivity equation at the previous time step for a given design velocity field. Using the same procedure as finite elasticity in Section 3.2, the sensitivity equation at the current configuration is obtained as

$$a^*_{\Omega}(\boldsymbol{z};\dot{\boldsymbol{z}},\bar{\boldsymbol{z}}) = \ell'_{\mathrm{V}}(\bar{\boldsymbol{z}}) - a'_{\mathrm{V}}(\boldsymbol{z},\bar{\boldsymbol{z}}), \quad \forall\,\bar{\boldsymbol{z}}\in Z \tag{74}$$

The linear system of Eq. (74) needs to be solved at each time step to compute the displacement sensitivity $\dot{\boldsymbol{z}}$. Note that the sensitivity equation of the classical rate-form plasticity provides the incremental displacement sensitivity whereas the sensitivity Eq. (74) provides the total displacement sensitivity even though Eq. (74) is solved at each time step.

After computing the displacement sensitivity $\dot{\boldsymbol{z}}$, the material derivatives of other path-dependent variables can be updated. The material derivative of the logarithmic principal stretch can be obtained from the definition of the strain and principal direction as

$$\dot{e}_j^{\mathrm{tr}} = \left(2\boldsymbol{F}^{\mathrm{e}}\frac{\partial e_j^{\mathrm{tr}}}{\partial\boldsymbol{C}^{\mathrm{e}}}\boldsymbol{F}^{\mathrm{e}^{\mathrm{T}}}\right) : (\boldsymbol{F}^{\mathrm{e}^{-\mathrm{T}}}\dot{\boldsymbol{E}}^{\mathrm{e}}\boldsymbol{F}^{\mathrm{e}^{-1}}) = \boldsymbol{m}^j : [\boldsymbol{\varepsilon}(\dot{\boldsymbol{z}}) + \boldsymbol{\varepsilon}_{\mathrm{V}}(\boldsymbol{z}) + \boldsymbol{\varepsilon}_{\mathrm{P}}(\boldsymbol{z})] \tag{75}$$

The material derivative of the unit normal vector to the yield surface and the plastic consistency parameter $\gamma$ can be obtained by differentiating Eqs. (13) and (14), respectively, as

$$\dot{\boldsymbol{N}} = \frac{1}{\|\boldsymbol{\eta}^{\mathrm{tr}}\|}(\boldsymbol{I}_{\mathrm{dev}} - \boldsymbol{N}\otimes\boldsymbol{N})(2\mu\dot{\boldsymbol{e}}^{\mathrm{tr}} - \dot{\boldsymbol{\alpha}}_n) \tag{76}$$

$$\dot{\gamma} = A\boldsymbol{N}^{\mathrm{T}}(2\mu\dot{\boldsymbol{e}}^{\mathrm{tr}} - \dot{\boldsymbol{\alpha}}_n) - A\kappa'\dot{e}_n^{\mathrm{p}} \tag{77}$$

Note that the local Newton's method is used to compute the plastic consistency parameter $\gamma$ for nonlinear hardening rule in response analysis whereas no iteration is required to compute $\dot{\gamma}$ in Eq. (77). By using Eqs. (76) and (77), $\dot{\boldsymbol{\alpha}}_n$ and $\dot{e}_n^{\mathrm{p}}$ are updated, using the same procedure as response analysis, as

$$\dot{\boldsymbol{\alpha}}_{n+1} = \dot{\boldsymbol{\alpha}}_n + \left(H_\alpha + \sqrt{\frac{2}{3}}H'_\alpha\gamma\right)\dot{\gamma} + H_\alpha\gamma\dot{\boldsymbol{N}} \tag{78}$$

$$\dot{e}_{n+1}^{\mathrm{p}} = \dot{e}_n^{\mathrm{p}} + \sqrt{\frac{2}{3}}\dot{\gamma} \tag{79}$$

The only thing left is the evaluation of the material derivative of deformation gradient $\boldsymbol{G}$ at the intermediate configuration, as given in Eq. (60). Since response analysis updates the symmetric left Cauchy–Green deformation tensor $\boldsymbol{b}^{\mathrm{e}} = \boldsymbol{F}^{\mathrm{e}}\boldsymbol{F}^{\mathrm{e}^{\mathrm{T}}}$ using Eq. (17), it is difficult to extract any information of $\boldsymbol{F}^{\mathrm{e}}$ or $\boldsymbol{F}^{\mathrm{p}}$ separately. In addition, it is difficult to express $\boldsymbol{G}$ in Eq. (60) in terms of $\boldsymbol{b}^{\mathrm{e}}$ and $\dot{\boldsymbol{b}}^{\mathrm{e}}$. From the updated Lagrangian formulation and the assumption of the isotropic material, the specification of the intermediate configuration is not necessary in response analysis. The intermediate configuration has an ambiguity up to the order of the rigid body rotation.

However, since $\dot{\boldsymbol{F}}^{\mathrm{p}}$ plays the role of the design velocity field at the intermediate configuration, it is necessary to

specify the intermediate configuration for DSA purposes. Without any loss of generality, it is possible to define the intermediate configuration as the unrotated de-stressing process (see Ref. [17]). By removing the rotational part from the polar decomposition of $\boldsymbol{F}^{\mathrm{e}} = \boldsymbol{V}^{\mathrm{e}}\boldsymbol{R}^{\mathrm{e}}$, the elastic deformation gradient can be obtained as

$$\boldsymbol{F}^{\mathrm{e}} \equiv \boldsymbol{V}^{\mathrm{e}} = \sqrt{\boldsymbol{b}^{\mathrm{e}}} \tag{80}$$

In this approach, the intermediate configuration defined by $\boldsymbol{F}^{\mathrm{p}}$ contains the rigid body rotation as well as the local de-stressing. Since the plastic evolution occurs on the principal logarithmic stretches of the current fixed configuration, the elastic deformation gradient $\boldsymbol{F}^{\mathrm{e}}$ and its design derivative can be expressed as

$$\boldsymbol{F}^{\mathrm{e}} = \sum_{i=1}^{3} \exp(e_i^{\mathrm{tr}} - \gamma N_i)\boldsymbol{m}^i \tag{81}$$

and

$$\dot{\boldsymbol{F}}^{\mathrm{e}} = \sum_{i=1}^{3} \exp(e_i^{\mathrm{tr}} - \gamma N_i)(\dot{e}_i^{\mathrm{tr}} - \dot{\gamma}N_i - \gamma\dot{N}_i)\boldsymbol{m}^i + \sum_{i=1}^{3} \exp(e_i^{\mathrm{tr}} - \gamma N_i)\hat{\boldsymbol{c}}^i : [\boldsymbol{\varepsilon}(\dot{\boldsymbol{z}}) + \boldsymbol{\varepsilon}_{\mathrm{V}}(\boldsymbol{z}) + \boldsymbol{\varepsilon}_{\mathrm{P}}(\boldsymbol{z})] \tag{82}$$

Finally, the material derivative of the intermediate configuration can be obtained as

$$\dot{\boldsymbol{F}}^{\mathrm{p}} = \boldsymbol{F}^{\mathrm{e}^{-1}}\dot{\boldsymbol{F}} - \boldsymbol{F}^{\mathrm{e}^{-1}}\dot{\boldsymbol{F}}^{\mathrm{e}}\boldsymbol{F}^{\mathrm{p}} \tag{83}$$

An interesting observation can be made by reducing the problems to elastic. If $\boldsymbol{F}^{\mathrm{e}} = \boldsymbol{F}$ and $\boldsymbol{F}^{\mathrm{p}} = \boldsymbol{I}$, then $\dot{\boldsymbol{F}}^{\mathrm{p}} = \boldsymbol{0}$ in Eq. (83) and the same structural fictitious load form as the finite elasticity in Eq. (55) is recovered. However, from the definition of $\boldsymbol{F}^{\mathrm{e}}$ in Eq. (82), $\boldsymbol{F}^{\mathrm{e}} = \boldsymbol{V}^{\mathrm{e}} \neq \boldsymbol{F}$, $\boldsymbol{F}^{\mathrm{p}} = \boldsymbol{R}^{\mathrm{e}}$, and $\dot{\boldsymbol{F}}^{\mathrm{p}} \neq \boldsymbol{0}$. Thus, the structural fictitious load form is different from that of the finite elasticity. This situation occurs because the intermediate configuration is different from the undeformed configuration even if the material is in elastic state. Thus, this type of decomposition is inappropriate from the DSA viewpoint even though response analysis yields an equivalent result as discussed by Simo [36]. The sensitivity of elastic rotation is not negligible and needs to be identified for sensitivity purpose. Note that the undeformed configuration cannot be recovered using the elastic deformation gradient in Eq. (80) even if no plastic deformation occurs.

To bring this inconsistency to a settlement, consider the return-mapping algorithm in Eq. (12) in the principal strain space. The logarithmic elastic principal stretch vector is updated by

$$\boldsymbol{e} = \boldsymbol{e}^{\mathrm{tr}} - \gamma\boldsymbol{N}, \quad \lambda_j^{\mathrm{e}} = \lambda_j^{\mathrm{e}^{\mathrm{tr}}} \exp(-\gamma N_j) \tag{84}$$

where $\exp(-\gamma N_j)$ is the principal value of incremental plastic deformation gradient $\boldsymbol{f}^{\mathrm{p}}$ with the current fixed principal direction. Thus, the incremental plastic deformation gradient is defined as

$$\boldsymbol{f}^{\mathrm{p}} = \sum_{j=1}^{3} \exp(-\gamma N_j)\boldsymbol{m}^j \tag{85}$$

and the updated elastic deformation gradient is

$$\boldsymbol{F}^{\mathrm{e}}_{n+1} = \boldsymbol{f}^{\mathrm{p}}\boldsymbol{F}^{\mathrm{e}^{\mathrm{tr}}}_{n+1} \tag{86}$$

Note that the incremental plastic deformation gradient $\boldsymbol{f}^{\mathrm{p}}$ in Eq. (85) is a symmetric tensor, which means the incremental plastic spin vanishes. From the relation of Eq. (1), the plastic deformation gradient is updated by

$$\boldsymbol{F}^{\mathrm{p}}_{n+1} = \boldsymbol{F}^{\mathrm{e}^{-1}}_{n+1}\boldsymbol{F}_{n+1} \tag{87}$$

and its material derivative is updated by

$$\dot{\boldsymbol{F}}^{\mathrm{p}}_{n+1} = \frac{\mathrm{d}}{\mathrm{d}\tau}(\boldsymbol{F}^{\mathrm{e}^{-1}}_{n+1})\boldsymbol{F}_{n+1} + \boldsymbol{F}^{\mathrm{e}^{-1}}_{n+1}\dot{\boldsymbol{F}}_{n+1} \tag{88}$$

where $\dot{\boldsymbol{F}}_{n+1}$ is given in Eq. (45) and

$$\frac{\mathrm{d}}{\mathrm{d}\tau}(\boldsymbol{F}^{\mathrm{e}^{-1}}_{n+1}) = -\boldsymbol{F}^{\mathrm{e}^{-1}}_{n+1}\dot{\boldsymbol{F}}^{\mathrm{e}}_{n+1}\boldsymbol{F}^{\mathrm{e}^{-1}}_{n+1}$$

with

$$\dot{\boldsymbol{F}}^{\mathrm{e}}_{n+1} = \dot{\boldsymbol{f}}^{\mathrm{p}}\boldsymbol{F}^{\mathrm{e}^{\mathrm{tr}}}_{n+1} + \boldsymbol{f}^{\mathrm{p}}\dot{\boldsymbol{F}}^{\mathrm{e}^{\mathrm{tr}}}_{n+1} \tag{89}$$

To show the consistency with the finite elastic state in the previous section, consider the elastic case, $\gamma = 0$, then $\boldsymbol{f}^{\mathrm{p}} = \boldsymbol{F}^{\mathrm{p}}_{n+1} = \boldsymbol{I}$ and $\dot{\boldsymbol{F}}^{\mathrm{p}}_{n+1} = 0$. Thus, the formulation exactly recovers the finite elasticity. It is shown that the intermediate configuration $\boldsymbol{F}^{\mathrm{p}}_{n+1}$ needs to be specified for the sensitivity purpose and is updated by removing the incremental plastic spin.

## 4. Numerical example: shape design sensitivity analysis and optimization of a bumper contact problem

Meshfree methods are developed in recent years to remove or reduce the mesh dependence of the conventional finite element method. In these methods, the shape function is not constructed from the reference domain but is formulated based on locations of material points. The order of completeness and the smoothness of the shape function can be easily changed. Insensitivity to the mesh distortion in these methods is a very important feature in nonlinear analysis and shape optimization. Higher accuracy can be achieved by adding nodes to the domain without remeshing. The domain is discretized by nonoverlapping regions (integration zone), and standard Gauss integration is used to evaluate the domain integral. This domain partitioning is independent to the nodal locations, and nodes are not

interconnected by elements. However, complexities in imposing the essential boundary condition and relatively high computational cost are weaknesses in these methods in spite of the aforementioned advantages. Some advances to resolve these difficulties have been developed [37,38]. For detailed discussions of meshfree methods, refer to Refs. [27–33,37,38]. For application of meshfree method to DSA, refer to Ref. [39].

The bumper of a vehicle is designed to protect the body from impact and to absorb the impact energy through the plastic deformation. The DOT regulation of the vehicle design requires that the bumper be able to sustain a 5-mph impact. In analysis, the bumper structure collides with a flat rigid wall. For DSA, the sensitivity coefficients of performance measures with respect to shape design parameters are computed. A DSA formulation of the contact problems developed by Kim et al. [39] is applied to this problem. Let $b_\Gamma(\boldsymbol{z},\bar{\boldsymbol{z}})$ and $b^*_\Gamma(\boldsymbol{z};\Delta\boldsymbol{z},\bar{\boldsymbol{z}})$ be the contact variational form and its linearization. Let denote the current time as $t_n$ and the iteration count as $k+1$, then the linearization of the structural variational equation including contact conditions becomes,

$$a^*_\Omega({}^n\boldsymbol{z}^k;\Delta\boldsymbol{z}^{k+1},\bar{\boldsymbol{z}})+b^*_\Gamma({}^n\boldsymbol{z}^k;\Delta\boldsymbol{z}^{k+1},\bar{\boldsymbol{z}})s = \ell_\Omega(\bar{\boldsymbol{z}})-a_\Omega({}^n\boldsymbol{z}^k,\bar{\boldsymbol{z}})-b_\Gamma({}^n\boldsymbol{z}^k,\bar{\boldsymbol{z}}),\quad \forall\bar{\boldsymbol{z}}\in Z \tag{90}$$

and the DSA equation becomes

$$a^*_\Omega(\boldsymbol{z};\dot{\boldsymbol{z}},\bar{\boldsymbol{z}})+b^*_\Gamma(\boldsymbol{z};\dot{\boldsymbol{z}},\bar{\boldsymbol{z}})=\ell'_{\mathrm{V}}(\bar{\boldsymbol{z}})-a'_{\mathrm{V}}(\boldsymbol{z},\bar{\boldsymbol{z}})-b'_{\mathrm{V}}(\boldsymbol{z},\bar{\boldsymbol{z}}),\quad \forall\bar{\boldsymbol{z}}\in Z \tag{91}$$

where $b'_{\mathrm{V}}(\boldsymbol{z},\bar{\boldsymbol{z}})$ is the contact fictitious load form presented in Ref. [39].

The cross-section of the metal bumper is modeled by 144 RKPM particles and 71 integration zones as shown in Fig. 3. Frictional contact conditions are established between the rigid wall and particles at the outer surface of the bumper with the contact penalty parameter $\omega_n=10^3$ and the friction coefficient $\mu=0.4$. The magnitude of $\omega_n$ is chosen such that $\omega_n$ has the same magnitude as the stiffness of the bumper. Finite deformation elastoplasticity with multiplicative decomposition of the deformation gradient is used as a constitutive model with Young's modulus $E=206.9$ GPa, Poisson's ratio $\nu=0.29$, plastic hardening modulus $H=1.1$ GPa, and initial yield stress $\sigma_{\mathrm{y}}=0.5$ GPa. Linear isotropic hardening is considered where the plastic consistency parameter can be solved explicitly without iteration.

The mounting points to the vehicle body are moved 2.8 cm toward the rigid wall. Nonlinear response analysis is carried out with 20 load steps using the standard Newton–Raphson method. After the solution is converged at each load step, the decomposed tangent stiffness matrix is stored for DSA, and following DSA, the

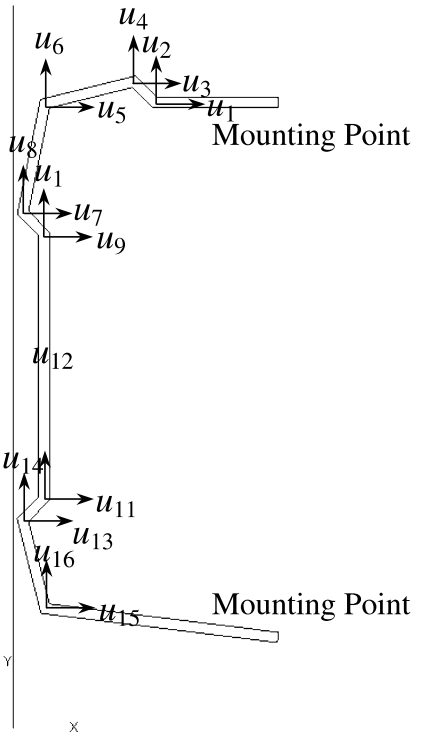


Fig. 3. Geometry and shape design parameterization of bumper contact problem.

intermediate configuration and internal plastic variables are updated. Fig. 4 shows the contour plots of the effective plastic strain and von Mises stress at the final converged configuration. The contact points moved outward as the deformation increases. Due to friction, the contact points do not move vertically. Excessive stress concentration and plastic strain are observed between the lower contact point and mounting point. These high stress and strain concentrations will be reduced through shape design changes.

Since a bumper is usually manufactured by a sheet-metal stamping process, it is inappropriate to change the thickness at each section in shape design optimization. The boundary of the bumper is represented by a cubic spline curve, and each particle point on the boundary has a unique parametric representation. The locations of the control points of each boundary curve are chosen as shape design parameters. The design velocity vector corresponding to the particle point can be computed using parametric representation. To maintain a constant thickness of 0.5 cm, design parameters corresponding to the inner/outer control points are retained in the thickness direction. Sixteen design parameters are chosen as shown in Fig. 3. After choosing the design parameters, the boundary design velocity field is obtained by perturbing the boundary curve in the direction of each

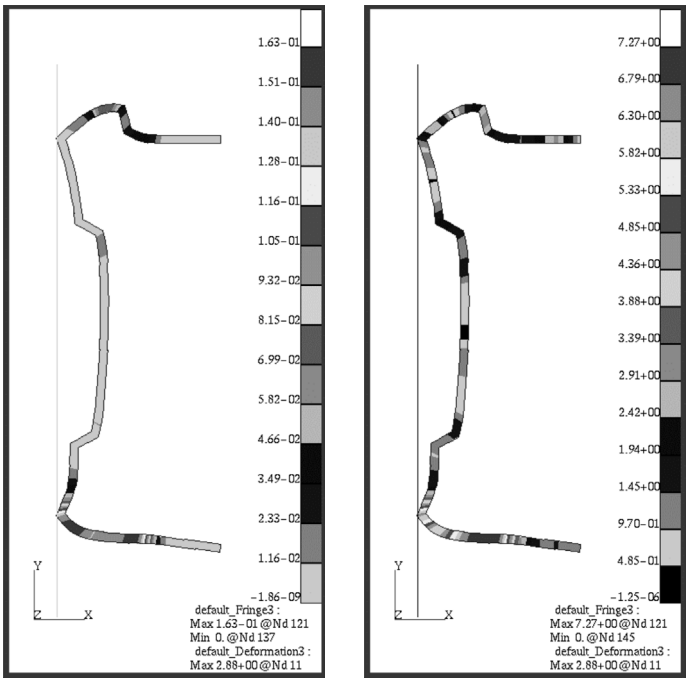


Fig. 4. Effective plastic strain and von Mises stress contour plots for bumper contact problem.

design parameters. Since all the particle points are on the boundary curve, the computation of the domain design velocity field is unnecessary. Refer to Ref. [40] for detailed explanation of the design velocity field.

Using the design velocity information, DSA is carried out. Since the constitutive model is based on the finite deformation elastoplasticity with multiplicative decomposition of the deformation gradient, the sensitivity formulation is path-dependent and is solved at each converged load step. The frictional contact also contributes to the path-dependency. After convergence in the response analysis at the current load step, the decomposed tangent stiffness matrix is stored for sensitivity analysis. Using the response analysis results, design velocity, and the material derivative of the intermediate configuration and internal plastic variables, the fictitious load form in Eq. (73) is computed. The linear system of Eq. (91) is solved using the decomposed tangent stiffness matrix obtained from response analysis with the fictitious load. No iteration is required to solve the sensitivity equation, but Eq. (91) is solved for the number of design parameters. Thus, the decomposition of tangent stiffness matrix is important. This procedure is quite efficient compared to iterative response analysis.

The design sensitivity equation is solved for the material derivative of the displacement $\dot{z}$. After computing $\dot{z}$, the material derivative of the intermediate configuration and internal plastic variables are updated using $\dot{z}$. The sensitivity coefficients of the performance measure are computed after solving the design sensitivity equation at the final converged load step. Possible performance measures are the displacement, stress tensor, internal variables, reaction force, contact force, and the normal gap distance. To show efficiency of the proposed method, the computation times of response analysis and DSA are compared. The response analysis is carried out with 275 s of CPU time. DSA takes 117 s for sixteen design parameters, which is less then 3% of the response analysis time per design parameter. This ratio is quite efficient compared to the finite difference method. This efficiency results from the fact that the sensitivity equation is solved without iteration and the decomposed tangent stiffness matrix from response analysis is used. Table 1 shows sensitivity coefficients and comparison of sensitivity results with finite difference results, and they agree extremely well. In Table 1, the third column $\Delta\Psi$ denotes the first order sensitivity results from the forward finite difference method with perturbation of $\tau = 10^{-6}$, and the fourth column represents the sensitivity computation results of the proposed method. In the first column, $z_x$, $e^{\mathrm{p}}$, and $F_{\mathrm{c}}$ are performance measures such as the displacement, effective plastic strain, and contact force, respectively. For example, $e^{\mathrm{p}}_{15}$ denotes the effective plastic strain at integration zone 15, and $F_{\mathrm{cx100}}$ denotes the $x$-directional contact force at the slave node 100.

Table 1
Comparison of design sensitivity results with finite difference method

| Performance ($\Psi$) | | $\Delta\Psi$ | $\Psi'$ | $(\Delta\Psi/\Psi') \times 100\%$ |
|---|---|---|---|---|
| $u_2$ | | | | |
| $e_{15}^{p}$ | 0.680005E − 01 | −0.179756E − 07 | −0.179757E − 07 | 100.00 |
| $e_{65}^{p}$ | 0.164338E + 00 | 0.311392E − 08 | 0.311393E − 08 | 100.00 |
| $e_{29}^{p}$ | 0.126643E − 01 | −0.901637E − 10 | −0.901545E − 10 | 100.01 |
| $z_{x39}$ | 0.429139E + 00 | 0.120943E − 06 | 0.120940E − 06 | 100.00 |
| $F_{cx100}$ | 0.379375E + 01 | 0.473864E − 07 | 0.473865E − 07 | 100.00 |
| $u_4$ | | | | |
| $e_{15}^{p}$ | 0.680005E − 01 | 0.246181E − 07 | 0.246181E − 07 | 100.00 |
| $e_{65}^{p}$ | 0.164338E + 00 | 0.105172E − 08 | 0.105173E − 08 | 100.00 |
| $e_{29}^{p}$ | 0.126643E − 01 | 0.589794E − 09 | 0.589795E − 09 | 100.00 |
| $z_{x39}$ | 0.429139E + 00 | −0.295825E − 06 | −0.295824E − 06 | 100.00 |
| $F_{cx100}$ | 0.379375E + 01 | 0.335517E − 09 | 0.335511E − 09 | 100.00 |
| $u_6$ | | | | |
| $e_{15}^{p}$ | 0.680005E − 01 | −0.170857E − 07 | −0.170857E − 07 | 100.00 |
| $e_{65}^{p}$ | 0.164338E + 00 | −0.237257E − 08 | −0.237256E − 08 | 100.00 |
| $e_{29}^{p}$ | 0.126643E − 01 | −0.720239E − 10 | −0.720198E − 10 | 100.01 |
| $z_{x39}$ | 0.429139E + 00 | 0.167699E − 06 | 0.167698E − 06 | 100.00 |
| $F_{cx100}$ | 0.379375E + 01 | −0.176290E − 07 | −0.176292E − 07 | 100.00 |
| $u_8$ | | | | |
| $e_{15}^{p}$ | 0.680005E − 01 | 0.581799E − 09 | 0.581877E − 09 | 99.99 |
| $e_{65}^{p}$ | 0.164338E + 00 | −0.635253E − 09 | −0.635254E − 09 | 100.00 |
| $e_{29}^{p}$ | 0.126643E − 01 | −0.185890E − 08 | −0.185890E − 08 | 100.00 |
| $z_{x39}$ | 0.429139E + 00 | −0.397143E − 07 | −0.397141E − 07 | 100.00 |
| $F_{cx100}$ | 0.379375E + 01 | 0.250196E − 07 | 0.250194E − 07 | 100.00 |
| $u_{10}$ | | | | |
| $e_{15}^{p}$ | 0.680005E − 01 | −0.262956E − 09 | −0.262932E − 09 | 100.01 |
| $e_{65}^{p}$ | 0.164338E + 00 | 0.136684E − 09 | 0.136687E − 09 | 100.00 |
| $e_{29}^{p}$ | 0.126643E − 01 | 0.873228E − 09 | 0.873231E − 09 | 100.00 |
| $z_{x39}$ | 0.429139E + 00 | −0.168128E − 06 | −0.168129E − 06 | 100.00 |
| $F_{cx100}$ | 0.379375E + 01 | −0.431408E − 07 | −0.431402E − 07 | 100.00 |

With safety consideration, a design optimization problem is formulated such that the area of the bumper cross-section is minimized with constraints on effective plastic strains. Since the impact condition is approximated by a quasistatic problem with the displacement driven method, equivalent inertia force is maintained by imposing constant normal force between the original and new designs through a design constraint. A design optimization problem with seven constraints on effective plastic strains and one constraint on the normal contact force is formulated as

$$\begin{aligned} &\text{minimize} && \text{Area} \\ &\text{subject to} && e_{16}^{p}(0.1) \leqslant 0.05, \quad e_{62}^{p}(0.15) \leqslant 0.05 \\ &&& e_{65}^{p}(0.16) \leqslant 0.05, \quad e_{66}^{p}(0.16) \leqslant 0.05 \\ &&& e_{67}^{p}(0.15) \leqslant 0.05, \quad e_{60}^{p}(0.15) \leqslant 0.05 \\ &&& e_{61}^{p}(0.14) \leqslant 0.05, \quad F_{cx}(4.55) \geqslant 4.55 \\ &&& -1.0 \leqslant u_i \leqslant 1.0 \quad i = 1, 16 \end{aligned} \tag{92}$$

The design optimization is carried out using the sequential quadratic programming (SQP) method in DOT [41]. The performance values are supplied to DOT from nonlinear response analysis (RKPM), and the sensitivity coefficients are provided by the proposed method. The initial design is infeasible, and all constraints on effective plastic strains are violated. The optimization is converged after 18 iterations and all constraints are satisfied. The cost function is reduced by 7% of the original value, and the normal contact force is slightly increased compared to the initial design. Fig. 5 shows the optimized shape design and the results of response analysis. Interestingly, the cross-section of bumper geometry is changed to somewhat symmetric shape even though the original design is not symmetric. The optimizer removed windings of the upper/lower parts because they are weak in bending type deformation. If a three-dimensional bumper is considered, the optimum shape is expected to be different from two-dimensional result.

Fig. 6 shows the iteration history of the cost function and constraints. After iteration number 5, no significant changes in the cost and constraints are observed.

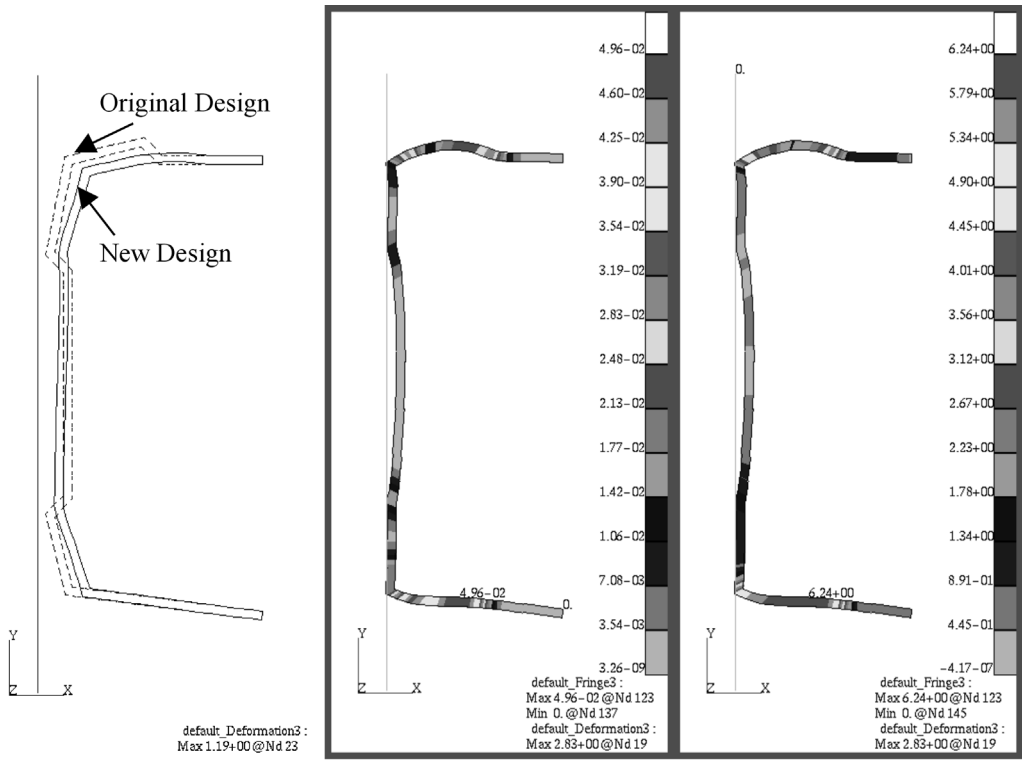


Fig. 5. Design optimization results of quasistatic bumper contact problem (a) optimized geometry, (b) effective plastic strain, (c) von Mises stress.

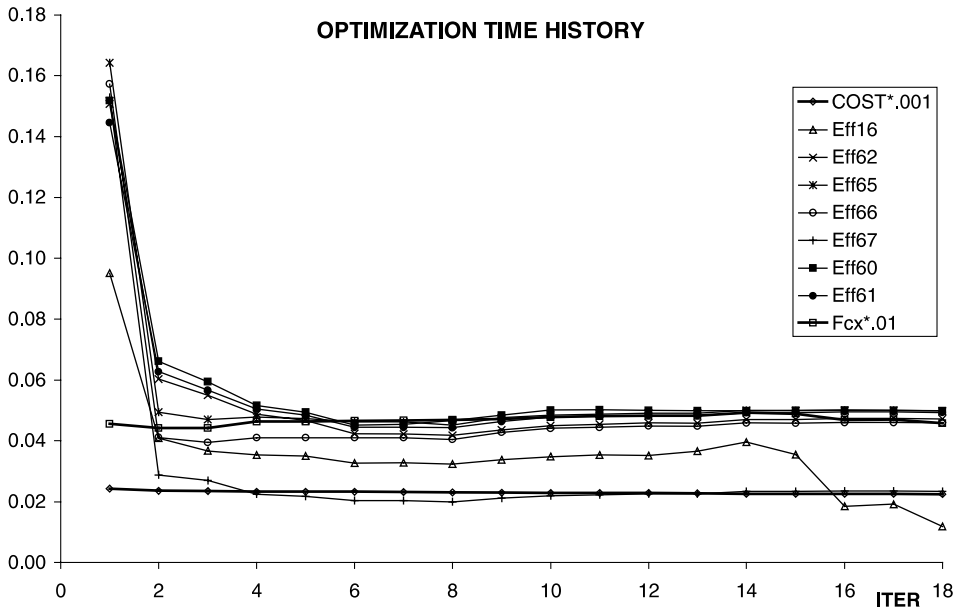


Fig. 6. Design optimization history for quasistatic bumper contact problem.

However, design parameters are changed relatively large during these iterations to find the optimum point. At the optimum design, six constraints on effective plastic strains and one constraint on the normal contact force are active.

## 5. Conclusions

Nonlinear shape DSA and optimization method for finite deformation elastoplastic structures with contact is developed using a continuum approach. The multiplicative decomposition of the deformation gradient and return mapping in the principal stress space are used. The difference of reference configurations between response analysis and DSA requires additional terms on the sensitivity equation, which represent the path-dependent effect. It is shown that the intermediate configuration needs to be specified for DSA purposes, which is not necessary in response analysis. The response analysis and DSA are carried out using the meshfree method (RKPM). The design sensitivity equation uses the same tangent stiffness as that of the response analysis, and thus no iteration is required to solve the design sensitivity equation at each converged load step for the path-dependent problem. The proposed DSA method is a very accurate and extremely efficient compared to the finite difference method.

## Acknowledgements

This research was partially supported by the NSF/DARPA OPAAL (DMS 98274015) and Ford University Research Program (URP 972723R). These supports are gratefully acknowledged.

## References

[1] Haug EJ, Choi KK, Komkov V. Design sensitivity analysis of structural systems. New York: Academic Press; 1986.
[2] Vidal CA, Haber RB. Design sensitivity analysis for rate-independent elastoplasticity. Comput Meth Appl Mech Engng 1993;107(3):393–431.
[3] Ohsaki M, Arora JS. Design sensitivity analysis of elastoplastic structures. Int J Numer Meth Engng 1994;37(5):737–62.
[4] Michaleris P, Tortorelli DA, Vidal CA. Tangent operators and design sensitivity formulations for transient nonlinear coupled problems with applications to elastoplasticity. Int J Numer Meth Engng 1994;37(14):2471–99.
[5] Lee TH, Arora JS. A computational method for design sensitivity analysis of elastoplastic structures. Comput Meth Appl Mech Engng 1995;122(1):27–50.
[6] Kleiber M, Kowalczyk P. Constitutive parameter sensitivity in elastoplasticity. Computat Mech 1995;17(1–2):36–48.
[7] Park YH, Choi KK. Design sensitivity analysis of truss structures with elastoplastic material. Mech Struct Machines 1996;24(2):189–216.
[8] Wiechmann W, Barthold FJ, Stein E. Optimization of elastoplastic structures using the finite element method. Proceedings of the Second World Congress of Structural and Multidisciplinary Optimization; 1997. p. 1013–8.
[9] Hughes TJR, Winget J. Finite rotation effects in numerical integration of rate constitutive equations arising in large-deformation analysis. Int J Numer Meth Engng 1980;15:1862–7.
[10] Zhang Q, Mukherjee S, Chandra A. Shape design sensitivity analysis for geometrically and materially nonlinear problems by the boundary element method. Int J Solids Struct 1992;29(2):2503–25.
[11] Dutta A. A study of implicit and explicit methods for design sensitivity analysis of nonlinear dynamic systems. PhD Thesis, Department of Civil and Environment Engineering, The University of Iowa, Iowa City, IA, 1996.
[12] Kleiber M. Shape and non-shape structural sensitivity analysis for problems with any material and kinematic nonlinearity. Comput Meth Appl Mech Engng 1993;108(1–2):73–97.
[13] Cho S, Choi KK. Design sensitivity analysis and optimization of nonlinear transient dynamics. Part II: configuration design. Int J Numer Meth Engng 2000;48(3):375–99.
[14] Maniatty AM, Chen MF. Shape sensitivity analysis for steady metal-forming processes. Int J Numer Meth Engng 1996;39(7):1199–217.
[15] Zhao GQ, Wright E, Grandhi RV. Preform die shape design in metal forming using an optimization method. Int J Numer Meth Engng 1997;40(7):1213–30.
[16] Balagangadhar D, Tortorelli DA. Design and analysis of large deformation continuous elastoplastic manufacturing processes via a steady displacement-based formulation. Seventh AIAA/USAF/NASA/ISSMO Symposium on Multidisciplinary Analysis and Optimization, St. Louise, MO, 1998. p. 1396–406.
[17] Lee EH. Elastic–plastic deformation at finite strains. J Appl Mech 1969;36:1–6.
[18] Asaro RJ. Micromechanics of crystals and polycrystals. Advances in applied mechanics. New York: Academic Press; 1983.
[19] Simo JC. Algorithms for static and dynamic multiplicative plasticity that preserve the classical return mapping schemes of the infinitesimal theory. Comput Meth Appl Mech Engng 1992;99(1):61–112.
[20] Moran B, Ortiz M, Shih CF. Formulation of implicit finite element methods for multiplicative finite deformation plasticity. Int J Numer Meth Engng 1990;29(3):483–514.
[21] Eterovic AL, Bathe KJ. A hyperelastic-based large strain elastoplastic constitutive formulation with combined isotropic–kinematic hardening using the logarithmic stress and strain measures. Int J Numer Meth Engng 1990;30(6):1099–114.
[22] Weber G, Anand L. Finite deformation constitutive equations and a time integration procedure for isotropic, hyperelastic–viscoplastic solids. Comput Meth Appl Mech Engng 1990;79(2):173–202.
[23] Miehe C, Stein E, Wagner W. Associative multiplicative elastoplasticity: formulation and aspects of the numerical

implementation including stability analysis. Comput Struct 1994;52(5):969–78.
[24] Simo JC, Hughes TJR. Computational inelasticity. New York: Springer; 1998.
[25] Badrinarayanan S, Zabaras N. A sensitivity analysis for the optimal design of metal-forming processes. Comput Meth Appl Mech Engng 1996;129(4):319–48.
[26] Wiechmann W, Barthold FJ. Remarks on variational design sensitivity analysis of structures with large elastoplastic deformations. Seventh AIAA/USAF/NASA/ISSMO Symposium on Multidisciplinary Analysis and Optimization; 1998. p. 349–58.
[27] Belytschko T, Lu YY, Gu L. Element free Galerkin method. Int J Numer Meth Engng 1994;37(2):229–56.
[28] Duarte CA, Oden JT. An h-p adaptive method using clouds. Comput Meth Appl Mech Engng 1996;139(1–4):237–62.
[29] Melenk JM, Babuska I. The partition of unity finite element method: basic theory and applications. Comput Meth Appl Mech Engng 1996;139(1–4):289–314.
[30] Liu WK, Jun S, Zhang YF. Reproducing kernel particle methods. Int J Numer Meth Fluids 1995;20(8–9):1081–106.
[31] Chen JS, Pan C, Wu CT, Liu WK. Reproducing kernel particle methods for large deformation analysis of nonlinear structures. Comput Meth Appl Mech Engng 1996; 139(1–4):195–227.
[32] Chen JS, Pan C, Roque C, Wang HP. A Lagrangian reproducing kernel particle method for metal forming analysis. Computat Mech 1998;22(3):289–307.
[33] Simo JC, Taylor RL. Quasi-compressible finite elasticity in principal stretches: continuum basis and numerical algorithms. Comput Meth Appl Mech Engng 1991;85(3):273–310.
[34] Choi KK, Santos JLT. Design sensitivity analysis of nonlinear structural systems. Part I: theory. Int J Numer Meth Engng 1987;24(11):2039–55.
[35] Santos JLT, Choi KK. Shape design sensitivity analysis of nonlinear structural systems. Struct Optimi 1992;4(1):23–35.
[36] Simo JC. On the computational significance of the intermediate configuration and hyperelastic stress relations in finite deformation elastoplasticity. Mech Mater 1985;4: 439–51.
[37] Chen JS, Wu CT, Yoon S, You Y. Stabilized conforming nodal integration for Galerkin meshfree methods. Int J Numer Meth Engng 2001;50(2):435–66.
[38] Chen JS, Wang HP. New boundary condition treatments for meshless computation of contact problems. Comput Meth Appl Mech Engng 2000;187(3–4):441–68.
[39] Kim NH, Choi KK, Chen JS, Park YH. Meshless shape design sensitivity analysis and optimization for contact problem with friction. Computat Mech 2000;25(2–3):157–68.
[40] Choi KK, Chang KH. A study on the velocity computation for shape design optimization. Finite Elem Anal Des 1994;15:317–47.
[41] Vanderplaats GN. DOT user's manual, VMA Corp., 1997, Colorado Springs, CO.